Applications of a new family of solutions of relativistic hydrodynamics

T. Csörgő[1,2] , G. Kasza[2], M. Csanád[3] and Z. Jiang[4,5]

[1]Wigner Research Center for Physics, Budapest, Hungary
[2]EKE GYKRC, Gyöngyös, Hungary
[3]Eötvös University, Budapest, Hungary
[4]Key Laboratory of Quark and Lepton Physics, Wuhan, China
[5]IoPP, CCNU, Wuhan, China

Introduction and motivation
A New Family of **Exact** Solutions of Relativistic Hydro
Rapidity and pseudorapidity distributions
Initial energy density
R_{long} HBT radius
Non-monotonic s-behaviour
Outlook
Conclusions, summary

A new family of exact solutions of relativistic hydrodynamics

T. Csörgő[1,2] , G. Kasza[2], M. Csanád[3] and Z. Jiang[4,5]

Introduction and motivation
A New Family of Exact Solutions of Relativistic Hydro
Rapidity and pseudorapidity distributions
R_{long} HBT radius
Outlook to other presentations
Conclusions, summary

arXiv.org:1805.01427 +

Partially supported by NKTIH FK 123842 and FK123959 and EFOP 3.6.1-16-2016-00001

Context

Renowned exact solutions, reviewed in arXiv:1805.01427

- **Landau-Khalatnikov solution: dn/dy ~ Gaussian**
- **Hwa solution (1974) – Bjorken: same solution + ε_0 (1983)**
- **Chiu, Sudarshan and Wang: plateaux, Wong: Landau revisited**

Revival of interest: Zimányi, Bondorf, Garpman (1978)
Buda-Lund model + exact solutions (1994-96)
Biró, Karpenko, Sinyukov, Pratt (2007)
Bialas, Janik, Peschanski, Borsch+Zhdanov (2007)
CsT, Csanád, Nagy (2007-2008)
CsT, Csernai, Grassi, Hama, Kodama (2004)
Gubser (2010-11)
Hatta, Noronha, Xiao (2014-16)

New simple solutions	→	**Evaluation of dn/dη**	arXiv:1806.06794
Rapidity distribution	→	**Advanced initial ε_0**	arXiv:1806.11309
HBT radii	→	**Advanced life-time τ_f**	arXiv:1810.00154
Energy scan	→	**Non-monotonic $\varepsilon_0(s)$**	arXiv:1811.0999

Goal

Need for solutions that are:

- **explicit**
- **simple**
- **accelerating**
- **relativistic**
- **realistic / compatible with the data:**
  - **lattice QCD EoS**
  - **ellipsoidal symmetry (spectra, v_2, v_4, HBT)**
  - **finite dn/dy**
- **Generelization of a class that satisfies each of these criteria but not simultaneously**

T. Cs, M. I. Nagy, M. Csanád, arXiv:nucl-th/0605070, PLB (2008)

M.I. Nagy, T. Cs., M. Csanád, arXiv:0709.3677 , PRC77:024908 (2008)

M. Csanád, M. I. Nagy, T. Cs, arXiv:0710.0327 [nucl-th] EPJ A (2008)

New family of exact solutions:

CsT, Kasza, Csanád, Jiang, arXiv.org:1805.01427

Perfect fluid hydrodynamics

Energy-momentum tensor:

$$T_{\mu\nu} = w u_\mu u_\nu - p g_{\mu\nu} \qquad w = \varepsilon + p$$

$$\partial_\nu T^{\mu\nu} = 0$$

Relativistic

Euler equation:

$$w u^\nu \partial_\nu u^\mu = \left(g^{\mu\rho} - u^\mu u^\rho\right) \partial_\rho p$$

Energy conservation:

$$w \partial_\mu u^\mu = -u^\mu \partial_\mu \varepsilon$$

Charge conservation:

$$\sum \mu_i \partial_\mu \left(n_i u^\mu\right) = 0$$

Consequence is entropy conservation:

$$\partial_\mu \left(\sigma u^\mu\right) = 0.$$

Self-similar, ellipsoidal solutions

Publication (for example):

T. Cs, L.P.Csernai, Y. Hama, T. Kodama, Heavy Ion Phys. A 21 (2004) 73

3D spherically symmetric HUBBLE flow:

$$u^\mu = \frac{x^\mu}{\tau}$$

No acceleration:

$$u^\mu \partial_\mu u_\nu = 0.$$

Define a scaling variable for self-similarly expanding ellipsoids:

$$s = \frac{r_x^2}{\dot{X}_0^2 t^2} + \frac{r_y^2}{\dot{Y}_0^2 t^2} + \frac{r_z^2}{\dot{Z}_0^2 t^2}$$

EoS: (massive) ideal gas

$$\epsilon = mn + \kappa p\,, \qquad p = nT.$$

$$\varepsilon_Q = m_Q n_Q + \lambda_\varepsilon n_Q T + B, \qquad p_Q = \lambda_p n_Q T - B,$$

$$n(t,\mathbf{r}) = n_0 \left(\frac{\tau_0}{\tau}\right)^3 \mathcal{V}(s) \qquad T(t,\mathbf{r}) = T_0 \left(\frac{\tau_0}{\tau}\right)^{3/\kappa} \frac{1}{\mathcal{V}(s)} \quad \Rightarrow \quad p(t,\mathbf{r}) = p_0 \left(\frac{\tau_0}{\tau}\right)^{3+3/\kappa}$$

Scaling function $\mathcal{V}(s)$ can be chosen freely.

Shear and bulk viscous corrections in NR limit: known analytically.

Auxiliary variables: η_x, τ, Ω , η_p, y

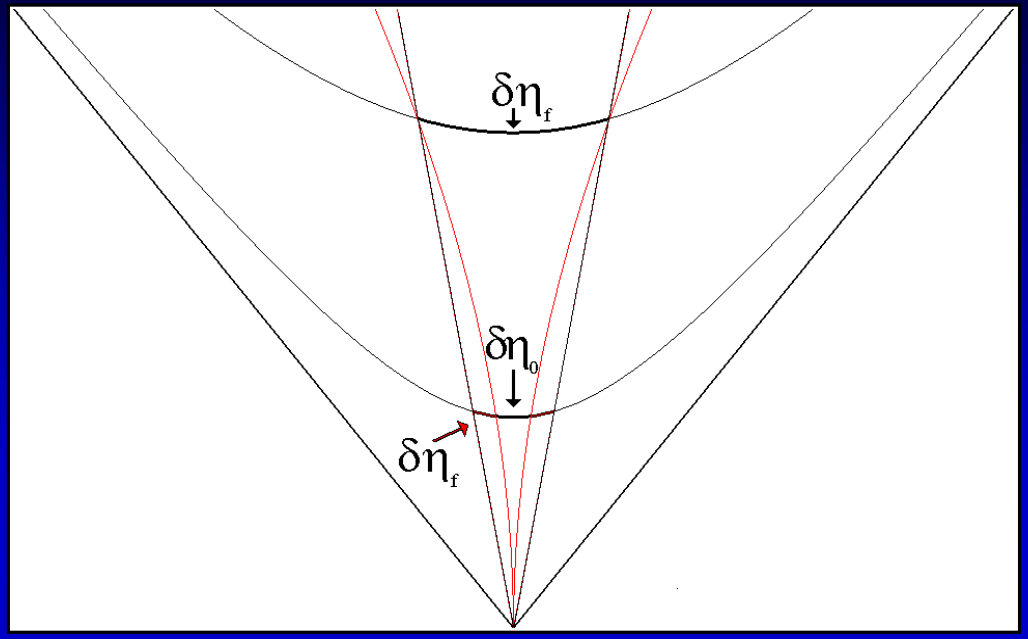

$$\tau = \sqrt{t^2 - r_z^2},$$

$$\eta_x = \frac{1}{2}\ln\left(\frac{t + r_z}{t - r_z}\right),$$

$$\Omega = \frac{1}{2}\ln\left(\frac{1 + v_z}{1 - v_z}\right).$$

$$u^\mu = (\cosh(\Omega), \sinh(\Omega)),$$

$$v_z = \tanh(\Omega).$$

$$\eta_p = \frac{1}{2}\ln\left(\frac{p + p_z}{p - p_z}\right),$$

$$y = \frac{1}{2}\ln\left(\frac{E + p_z}{E - p_z}\right),$$

Consider a 1+1 dimensional, finite, expanding fireball

Assume: $\Omega=\Omega(\eta_x)$

Notation T. Cs., G. Kasza, M. Csanád, Z. Jiang, arXiv.org:1805.01427

Hydro in Rindler coordinates, new sol

$$\partial_\nu T^{\mu\nu} = 0,$$
$$\partial_\mu (\sigma u^\mu) = 0,$$

Assumptions of TCs, Kasza, Csanád and Jiang, arXiv.org:1805.01427 :

$$\Omega = \Omega(\eta_x), \qquad \varepsilon = \kappa p, \qquad p = \frac{T\sigma}{1+\kappa}.$$

For the entropy density, the continuity equation is solved.

From energy-momentum conservation, the Euler and temperature equations are obtained:

$$\partial_{\eta_x}\Omega + \kappa\left(\tau\partial_\tau + \tanh(\Omega-\eta_x)\partial_{\eta_x}\right)\ln(T) = 0,$$
$$\partial_{\eta_x}\ln(T) + \tanh(\Omega-\eta_x)\left(\tau\partial_\tau \ln(T) + \partial_{\eta_x}\Omega\right) = 0.$$

A New Family of Exact Solutions of Hydro

$$
\begin{aligned}
\eta_x(H) &= \Omega(H) - H, \\
\Omega(H) &= \frac{\lambda}{\sqrt{\lambda-1}\sqrt{\kappa-\lambda}} \arctan\left(\sqrt{\frac{\kappa-\lambda}{\lambda-1}}\tanh(H)\right), \\
\sigma(\tau,H) &= \sigma_0\left(\frac{\tau_0}{\tau}\right)^{\lambda} \mathcal{V}_\sigma(s)\left[1+\frac{\kappa-1}{\lambda-1}\sinh^2(H)\right]^{-\frac{\lambda}{2}}, \\
T(\tau,H) &= T_0\left(\frac{\tau_0}{\tau}\right)^{\frac{\lambda}{\kappa}} \mathcal{T}(s)\left[1+\frac{\kappa-1}{\lambda-1}\sinh^2(H)\right]^{-\frac{\lambda}{2\kappa}}, \\
\mathcal{T}(s) &= \frac{1}{\mathcal{V}_\sigma(s)}, \\
s(\tau,H) &= \left(\frac{\tau_0}{\tau}\right)^{\lambda-1} \sinh(H)\left[1+\frac{\kappa-1}{\lambda-1}\sinh^2(H)\right]^{-\lambda/2}.
\end{aligned}
$$

$$u_\mu \partial^\mu s = 0.$$

A New Family of Exact Solutions of Hydro

$$
\begin{aligned}
\eta_x(H) &= \Omega(H) - H, \\
\Omega(H) &= \frac{\lambda}{\sqrt{\lambda-1}\sqrt{\kappa-\lambda}} \arctan\left(\sqrt{\frac{\kappa-\lambda}{\lambda-1}}\tanh(H)\right), \\
\sigma(\tau,H) &= \sigma_0\left(\frac{\tau_0}{\tau}\right)^{\lambda} \mathcal{V}_\sigma(s)\left[1+\frac{\kappa-1}{\lambda-1}\sinh^2(H)\right]^{-\frac{\lambda}{2}}, \\
T(\tau,H) &= T_0\left(\frac{\tau_0}{\tau}\right)^{\frac{\lambda}{\kappa}} \mathcal{T}(s)\left[1+\frac{\kappa-1}{\lambda-1}\sinh^2(H)\right]^{-\frac{\lambda}{2\kappa}}, \\
\mathcal{T}(s) &= \frac{1}{\mathcal{V}_\sigma(s)}, \qquad u_\mu \partial^\mu s = 0. \\
s(\tau,H) &= \left(\frac{\tau_0}{\tau}\right)^{\lambda-1} \sinh(H)\left[1+\frac{\kappa-1}{\lambda-1}\sinh^2(H)\right]^{-\lambda/2}.
\end{aligned}
$$

New feature:
Solution is given
as *parametric curves of H* in η_x :
$(\eta_x(H),\Omega(H,\tau))$
Simlification, for now:
limit the solution in η_x
where parametric curves
correspond to *functions*

New: not discovered before, as far as we know …

Family:
For each positive scaling function $\tau(s)$, a different solution, with same T_0, s_0, κ, λ

Not self-similar:
Coordinate dependenc NOT on scaling variable s ONLY, but additional dependence on $H = H(\eta_x)$ too.

Explicit and Exact:
Fluid rapidity, temperature, entropy density explicitly given by formulas

Limited in space-time rapidity η_x

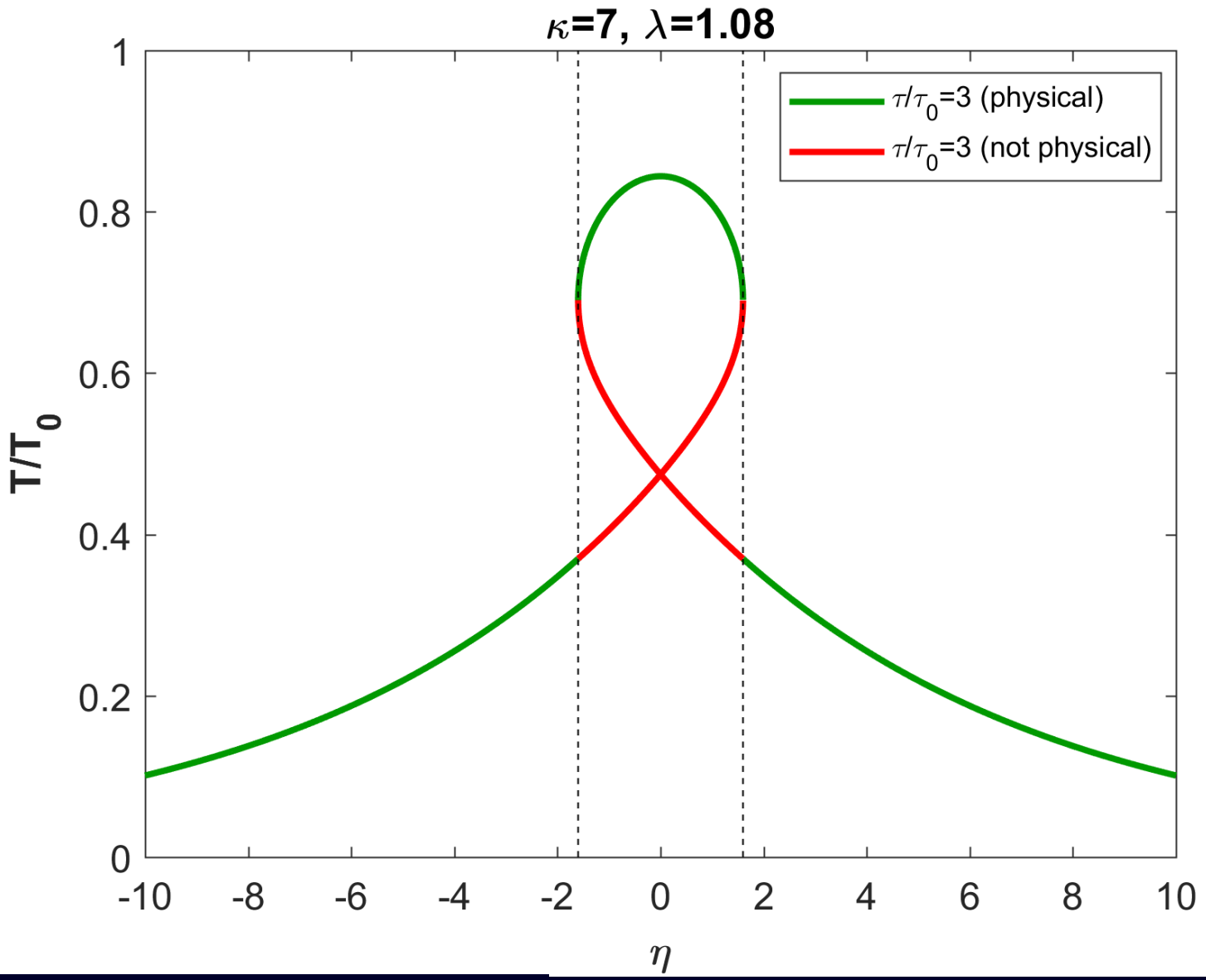

$$\left(\frac{1}{\sqrt{\kappa}}\right),$$

$$\left(\frac{1}{\sqrt{\kappa}}\right),$$

$$|\eta_{max}|)\Big),$$

Illustration: results for T

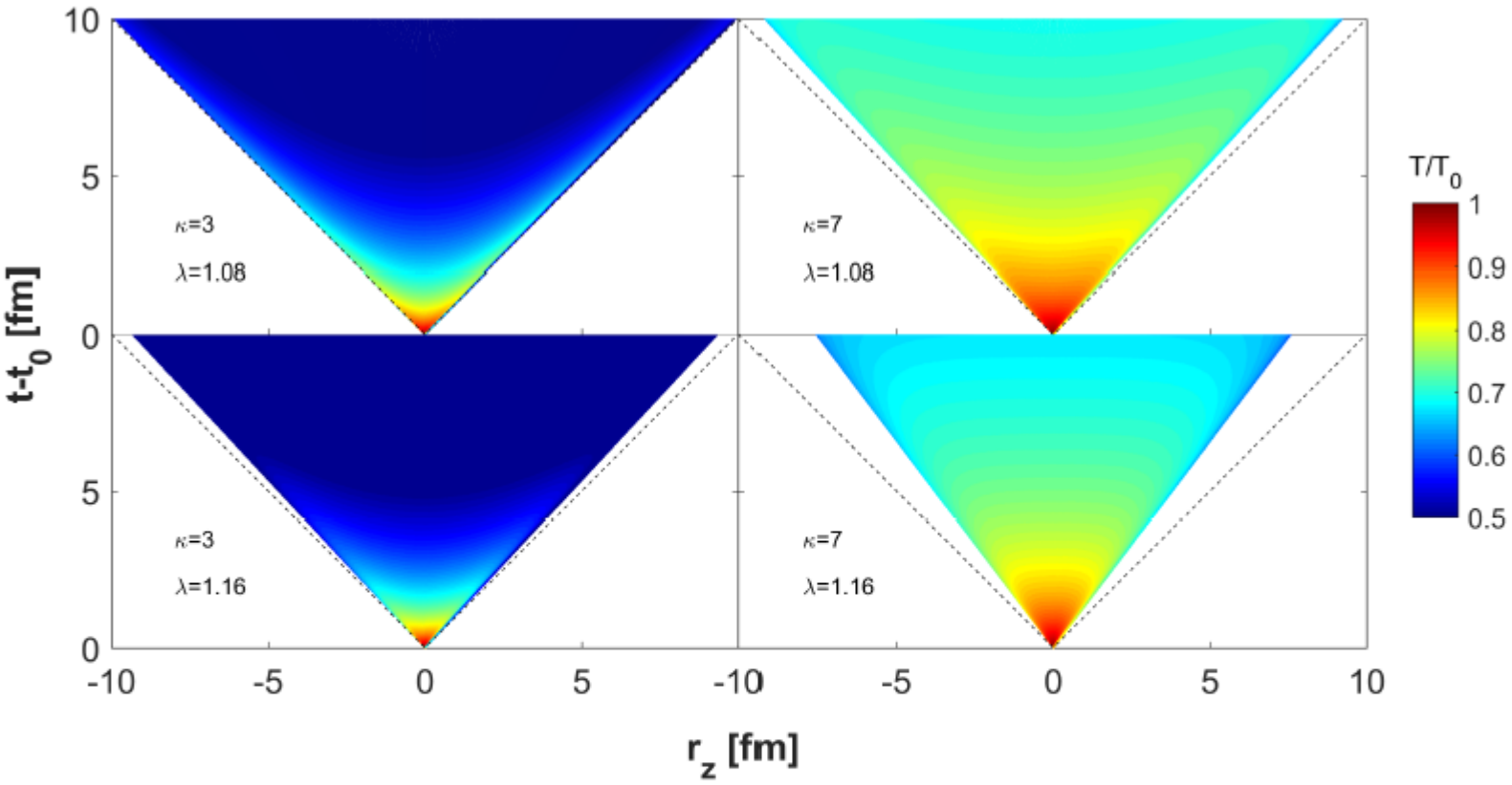

Figure 1. Temperature maps in the forward light cone from our new, longitudinally finite solutions for $\kappa = \varepsilon/p = 3$ (left column) and for $\kappa = 7$ (right column) evaluated for the acceleration parameters $\lambda = 1.08$ (top row) corresponding to a broader rapidity distribution and for $\lambda = 1.16$ (bottom row) corresponding to a narrower rapidity distribution, approximately corresponding to heavy ion collisions at $\sqrt{s_{NN}} = 200$ GeV RHIC and $\sqrt{s_{NN}} = 2.76$ TeV LHC energies.

Limited in space-time rapidity η_x

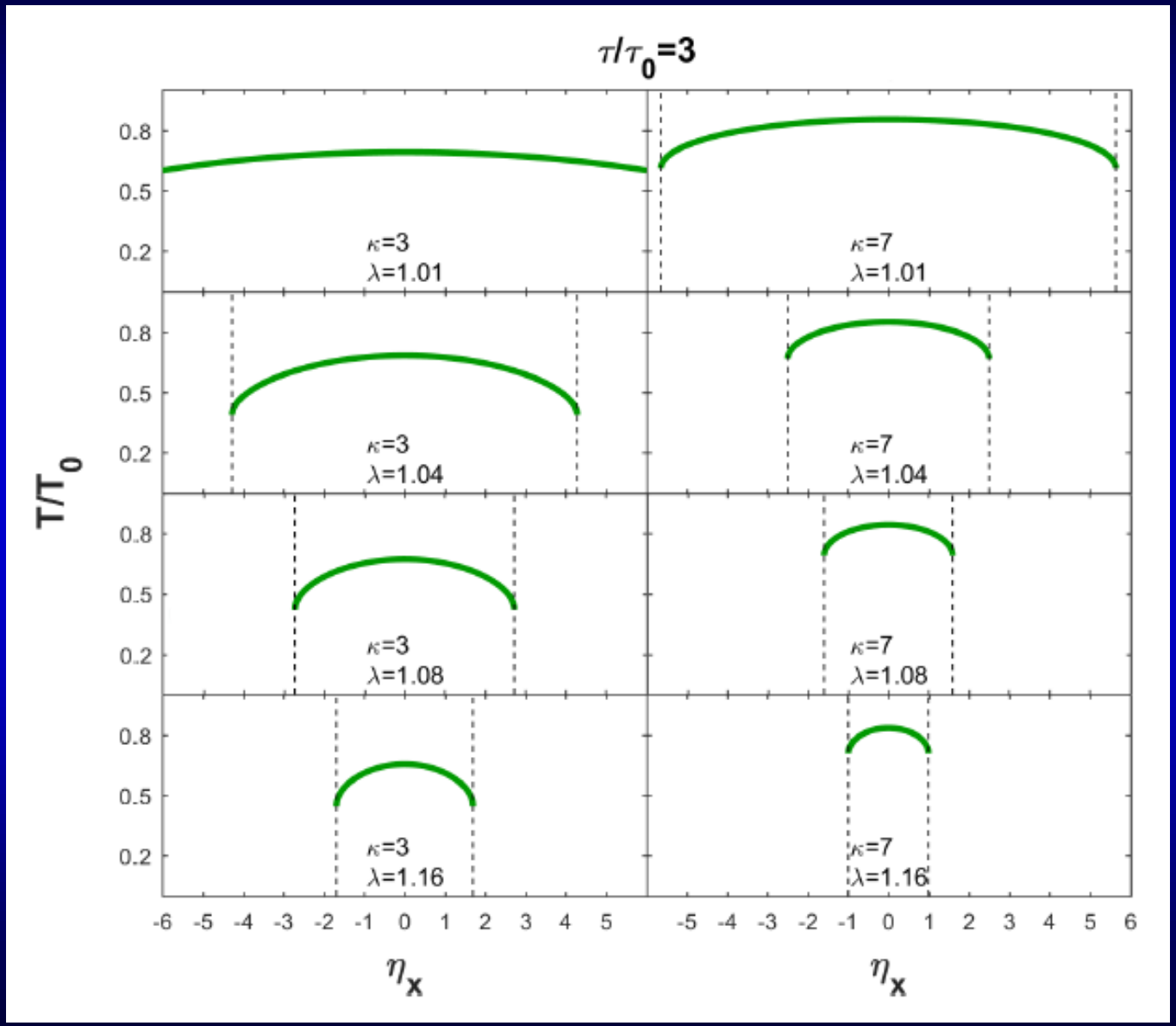

Illustration: results for fluid rapidity Ω

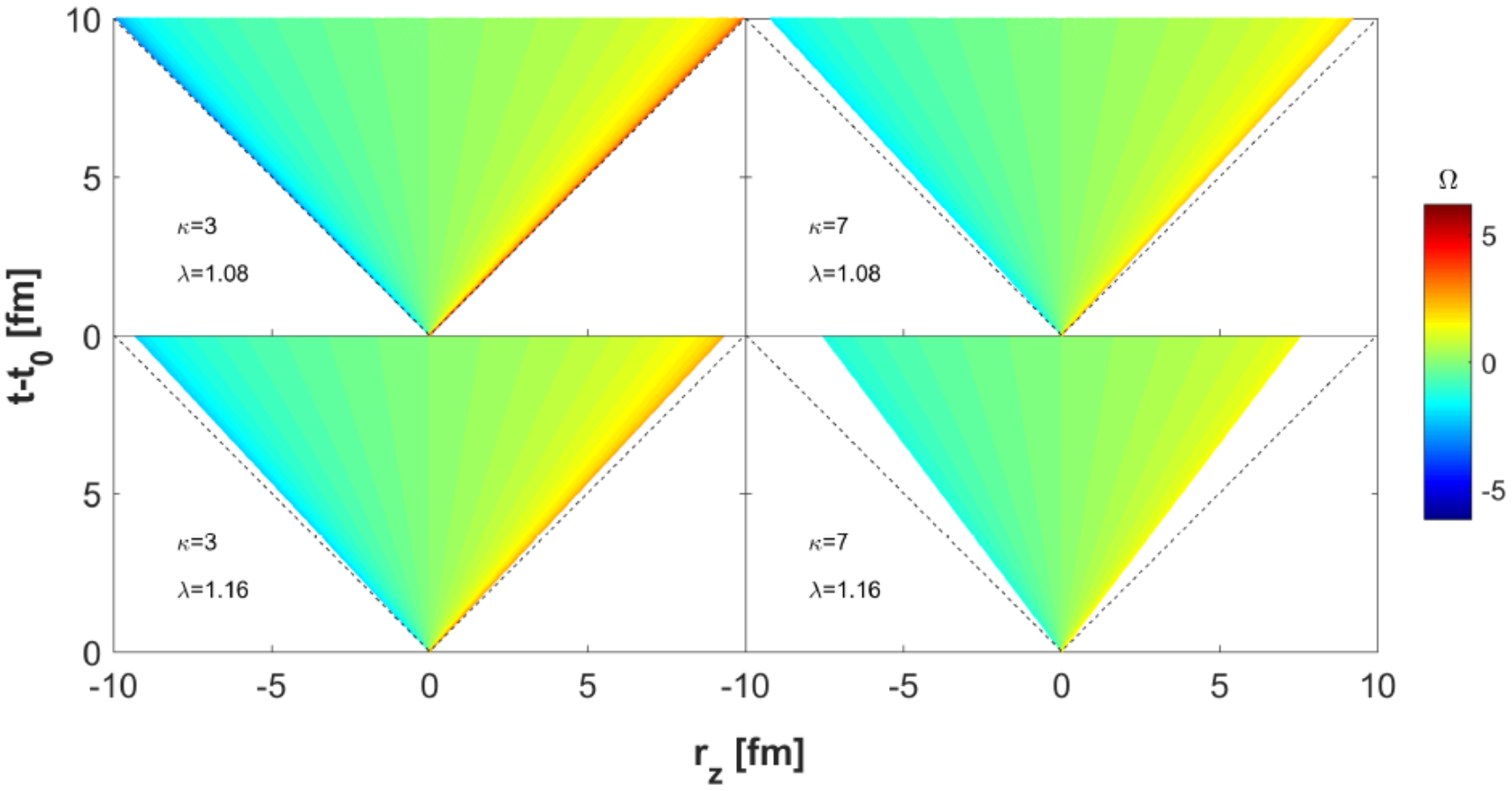

Figure 3. Fluid rapidity Ω maps in the forward light cone from our new, longitudinally finite solutions are shown for for $\kappa = \varepsilon/p = 3$ (left column) and for $\kappa = 7$ (right column) evaluated for the acceleration parameters $\lambda = 1.01$, 1.02, 1.04 and 1.08 (from top to bottom rows) corresponding to nearly flat and with increasing λ, gradually narrowing rapidity distributions.

Limited in space-time rapidity η_x

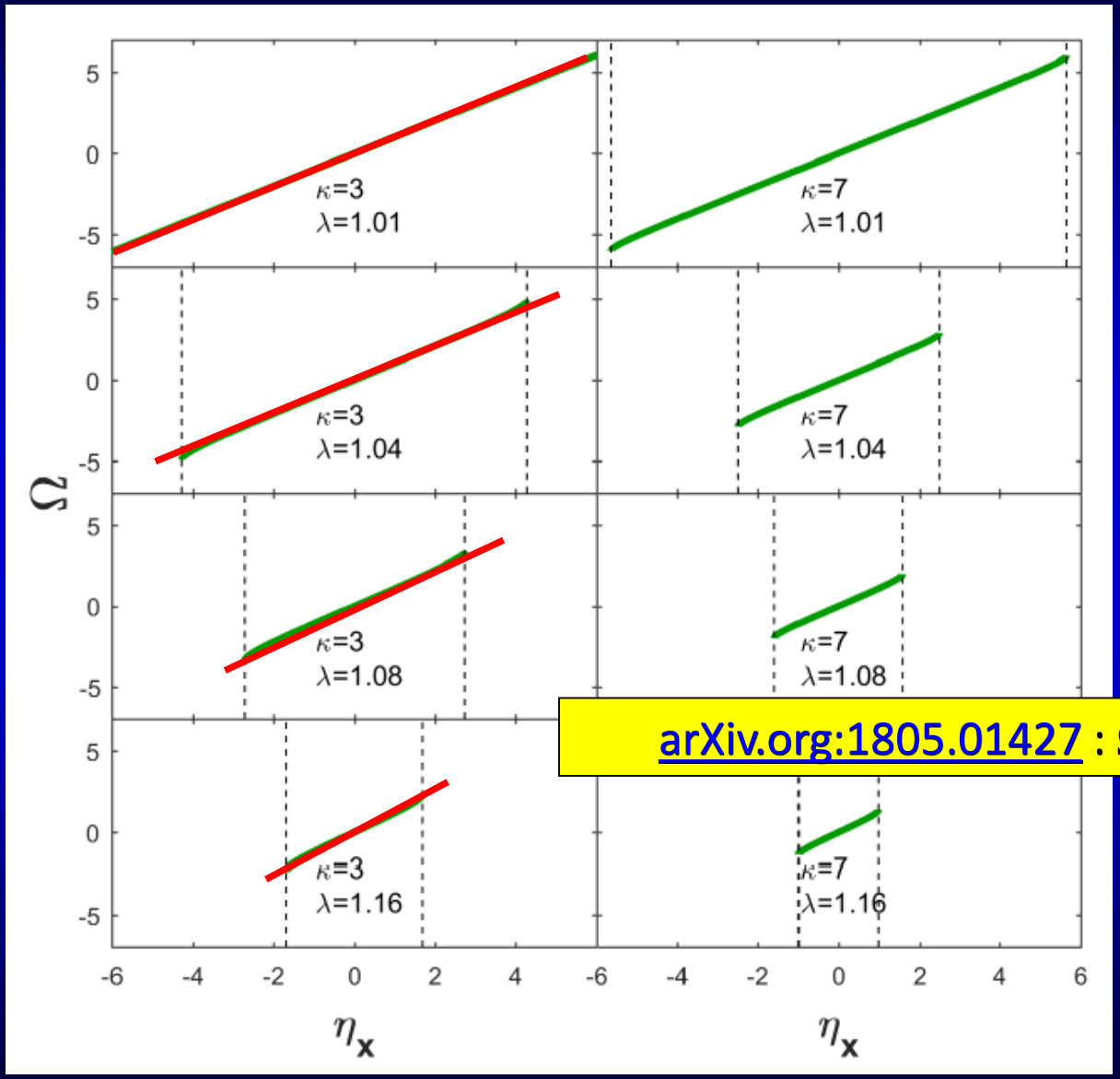

arXiv.org:1805.01427 : $\Omega \approx \lambda \eta_x$

Approximations near midrapidity

$$\frac{1-\kappa\tanh^2(\Omega-\eta_s)}{1-\tanh^2(\Omega-\eta_s)}\Omega' = \lambda,$$

$$\Rightarrow \quad \Omega' = \lambda\frac{1-\tanh^2(\Omega-\eta_s)}{1-\kappa\tanh^2(\Omega-\eta_s)},$$

$$\Rightarrow \quad \eta_s = -H + \frac{\lambda}{\sqrt{\lambda-1}\sqrt{\kappa-\lambda}}\mathrm{Arctan}\left(\sqrt{\frac{\kappa-\lambda}{\lambda-1}}\tanh(H)\right).$$

$$H = \Omega - \eta_s \ll 1,\ \kappa > 1,\ \lambda > 1,$$

$$T = T_i\left(\frac{\widetilde{\tau}_0}{\tau}\right)^{\frac{\lambda}{\kappa}}\exp\left[-\frac{\lambda(\lambda-1)(\kappa-1)}{2\kappa}\eta_s^2\right],$$

$$H = \Omega - \eta_s \ll 1,$$

$$\mathrm{Arctan}\left(\sqrt{\frac{\kappa-\lambda}{\lambda-1}}\tanh(H)\right) \simeq \sqrt{\frac{\kappa-\lambda}{\lambda-1}}H,$$

$$\Rightarrow \quad H = (\lambda-1)\eta_s,$$

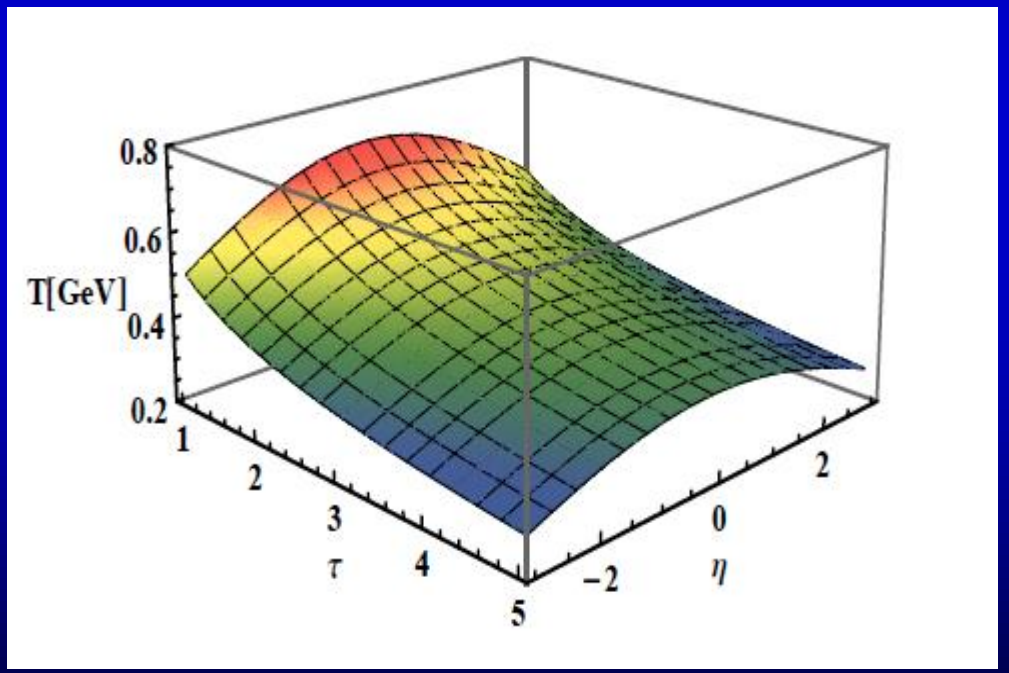

Observables: rapidity distribution

$$d\sigma^{\mu} = \frac{1}{A(\eta_x)}\left(\partial_{\eta_x} r_z,\, \partial_{\eta_x} t\right) d\eta_x,$$

$$\frac{\tau(H)}{\tau_f} = \cosh^{\frac{\kappa}{\lambda-\kappa}}(H)\left[1+\frac{\kappa-1}{\lambda-1}\sinh^2(H)\right]^{\frac{\lambda}{2(\kappa-\lambda)}}.$$

dn/dy evaluated analytically, in a saddle-point approximation

$$\frac{dn}{dy} \approx \left.\frac{dn}{dy}\right|_{y=0} \cosh^{-\frac{1}{2}\alpha(\kappa)-1}\left(\frac{y}{\alpha(1)}\right) \exp\left(-\frac{m}{T_f}\left[\cosh^{\alpha(\kappa)}\left(\frac{y}{\alpha(1)}\right)-1\right]\right),$$

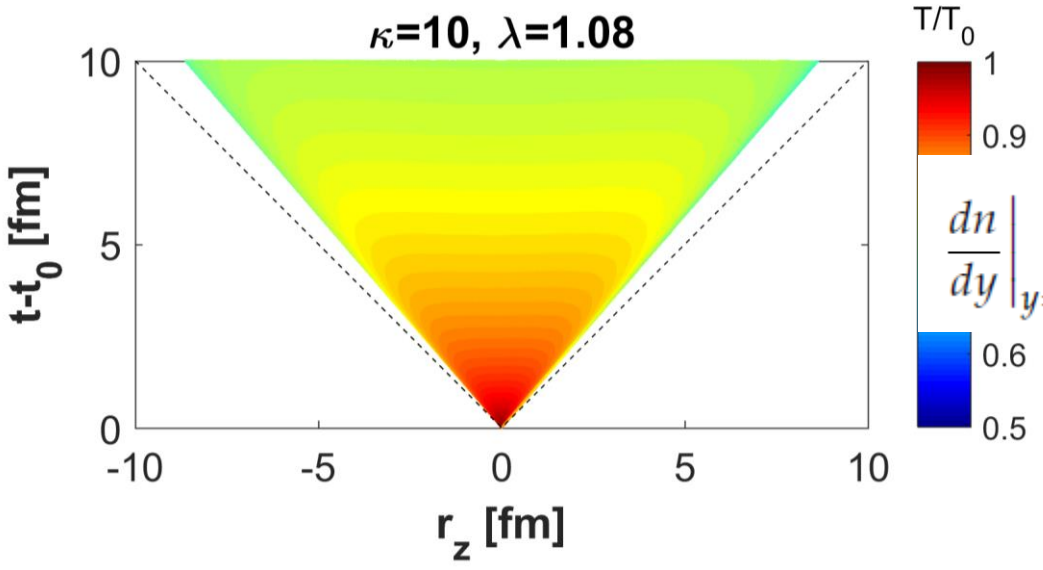

$$\alpha(\kappa) = \frac{2\lambda-\kappa}{\lambda-\kappa}.$$

$$\left.\frac{dn}{dy}\right|_{y=0} = \frac{R^2\pi\tau_f}{(2\pi\hbar)^3}\sqrt{\frac{(2\pi T_f m)^3}{\lambda(2\lambda-1)}}\exp\left(-\frac{m}{T_f}\right),$$

Pseudorapidity distribution

dn/dη evaluated analytically, in an advanced saddle-point approximation

$$\frac{dn}{dy} \approx \left.\frac{dn}{dy}\right|_{y=0} \cosh^{-\frac{1}{2}\alpha(\kappa)-1}\left(\frac{y}{\alpha(1)}\right) \exp\left(-\frac{m}{T_f}\left[\cosh^{\alpha(\kappa)}\left(\frac{y}{\alpha(1)}\right)-1\right]\right),$$

$$\left.\frac{dn}{dy}\right|_{y=0} = \frac{R^2\pi\tau_f}{(2\pi\hbar)^3}\sqrt{\frac{(2\pi T_f m)^3}{\lambda(2\lambda-1)}}\exp\left(-\frac{m}{T_f}\right), \qquad \alpha(\kappa) = \frac{2\lambda-\kappa}{\lambda-\kappa}.$$

$$\frac{dn}{d\eta_p} \approx \left.\frac{dn}{dy}\right|_{y=0} \frac{\langle p_T(y)\rangle \cosh(\eta_p)}{\sqrt{m^2+\langle p_T(y)\rangle^2\cosh(\eta_p)}} \cosh^{-\frac{1}{2}\alpha(\kappa)-1}\left(\frac{y}{\alpha(1)}\right) \exp\left(-\frac{m}{T_f}\left[\cosh^{\alpha(\kappa)}\left(\frac{y}{\alpha(1)}\right)-1\right]\right),$$

$$\langle p_T(y)\rangle \approx \frac{\sqrt{T_f^2+2mT_f}}{1+\frac{\alpha(\kappa)}{2\alpha(1)^2}\frac{T_f+m}{T_f+2m}y^2}.$$

An important by-product: $\langle p_T \rangle = \langle p_T(y) \rangle$ is rapidity dependent, a Lorentzian just as in Buda-Lund model

dn/dη for p+p, 7-8 TeV, CMS data

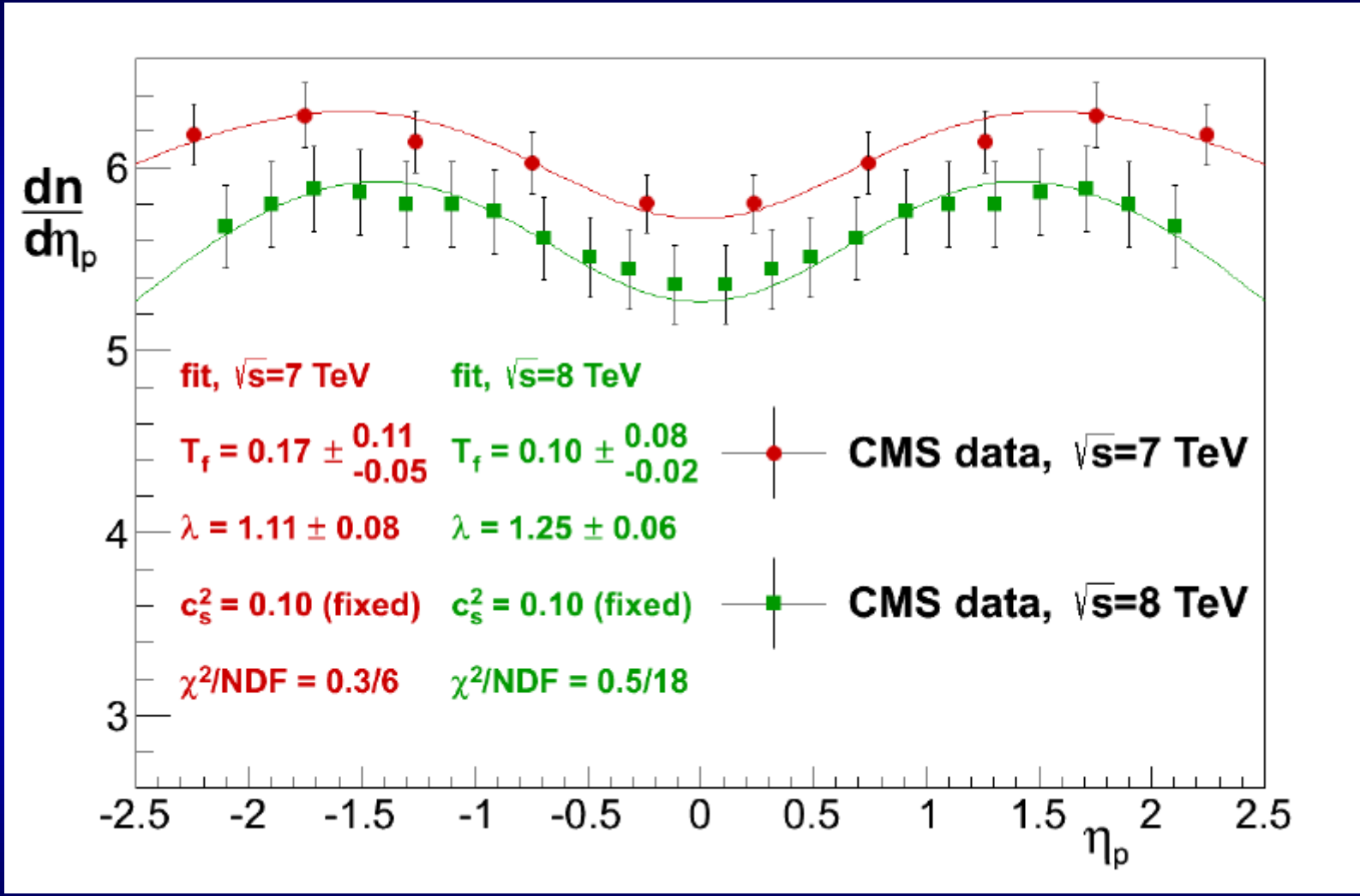

arXiv.org:1805.01427

dn/dη for Pb+Pb, 5 TeV, ALICE data

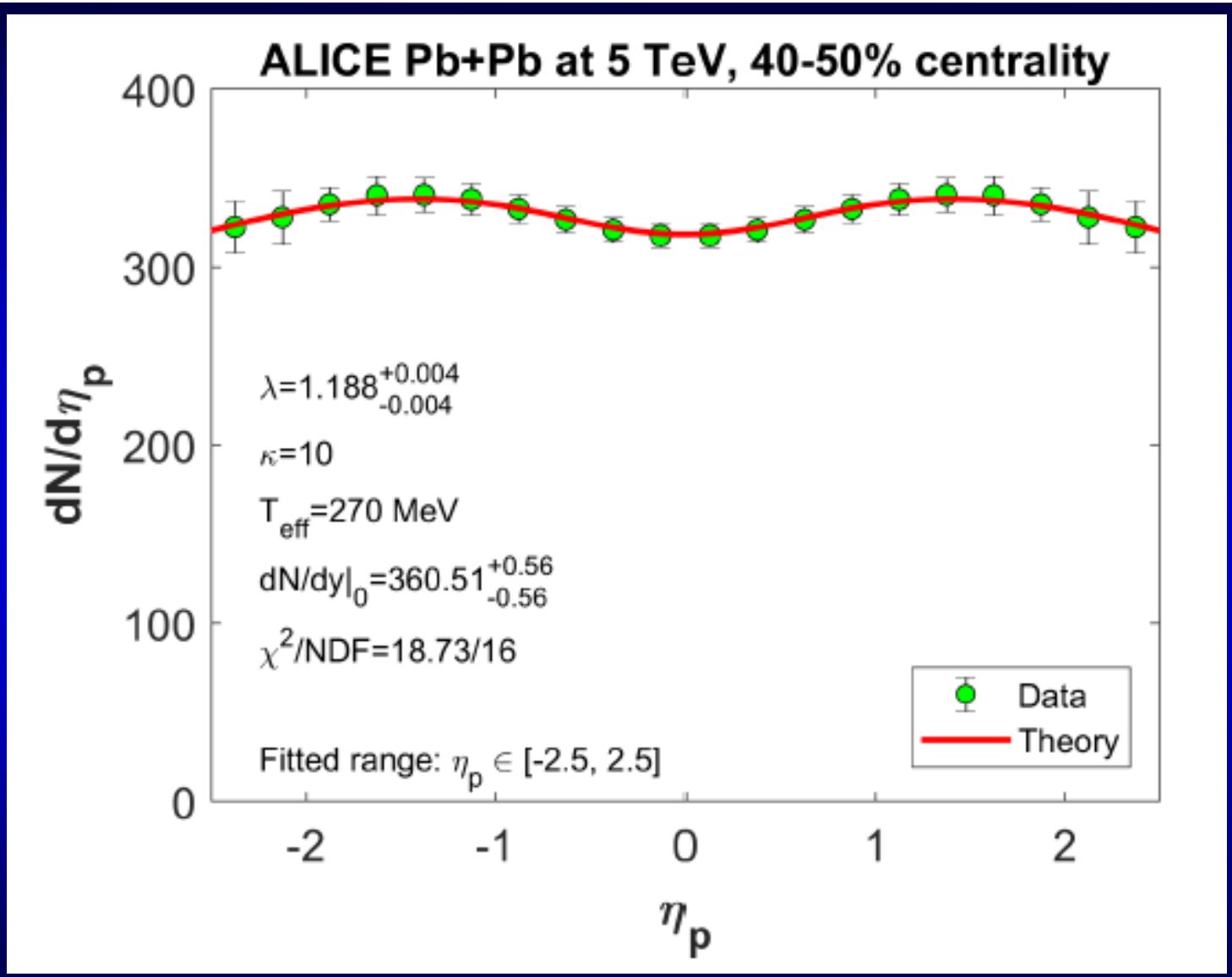

arXiv.org:1806.06794

dn/dη for Xe+Xe, 5.44 TeV, CMS data

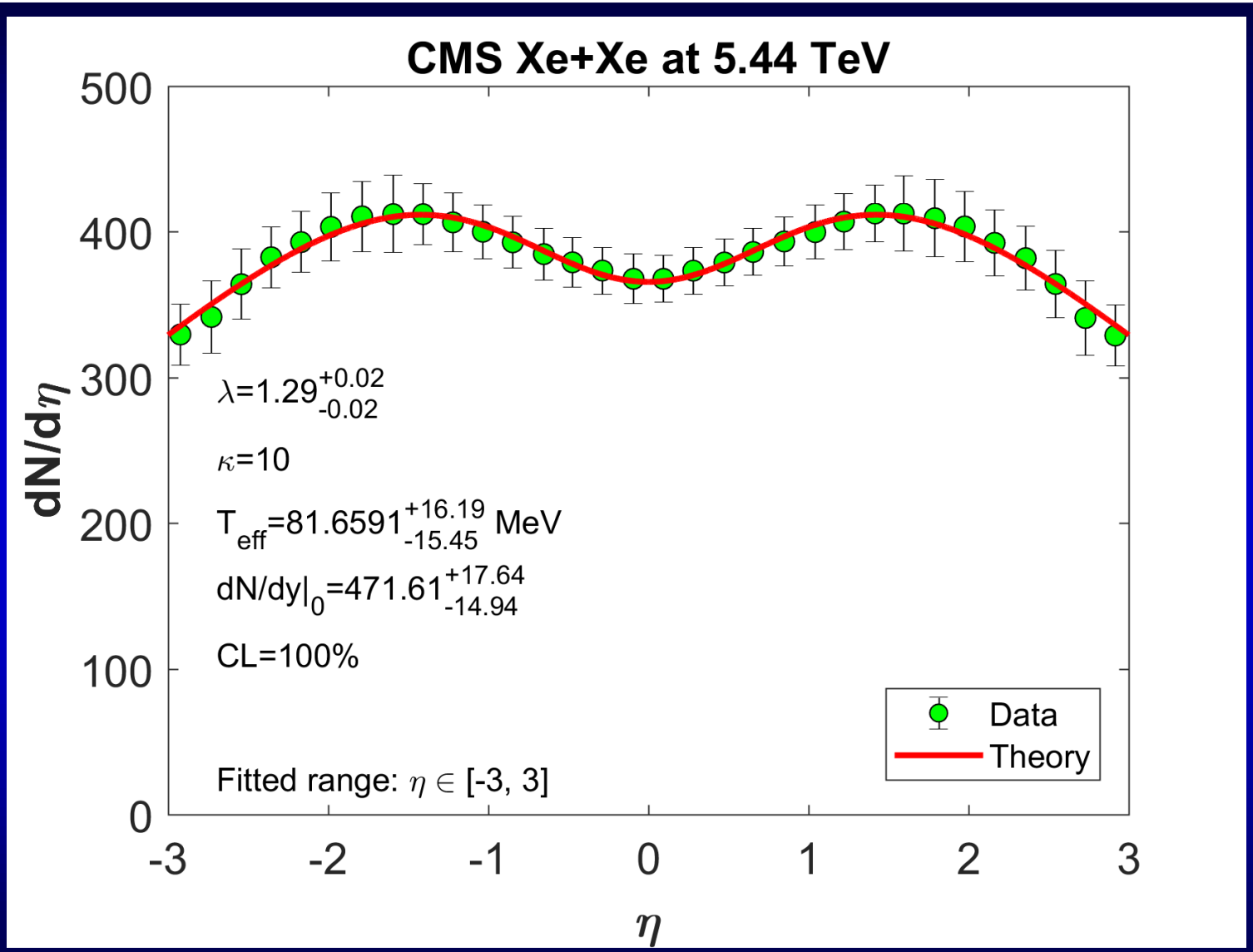

NEW (preliminary, too good)

dn/dη for Au+Au, 200 GeV, PHOBOS

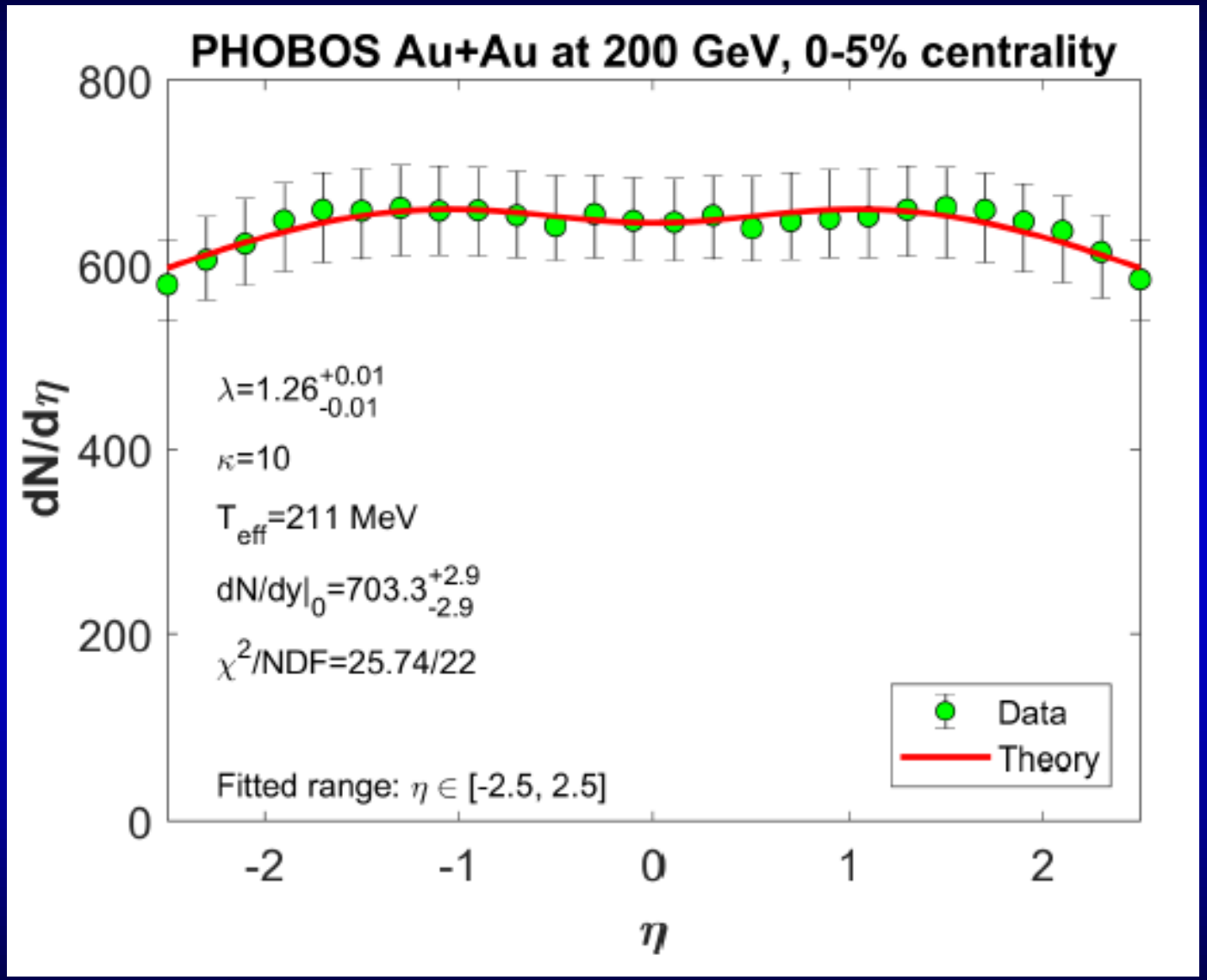

arXiv.org:1806.11309

dn/dη fits, $\sqrt{s_{NN}}$ = 200 GeV

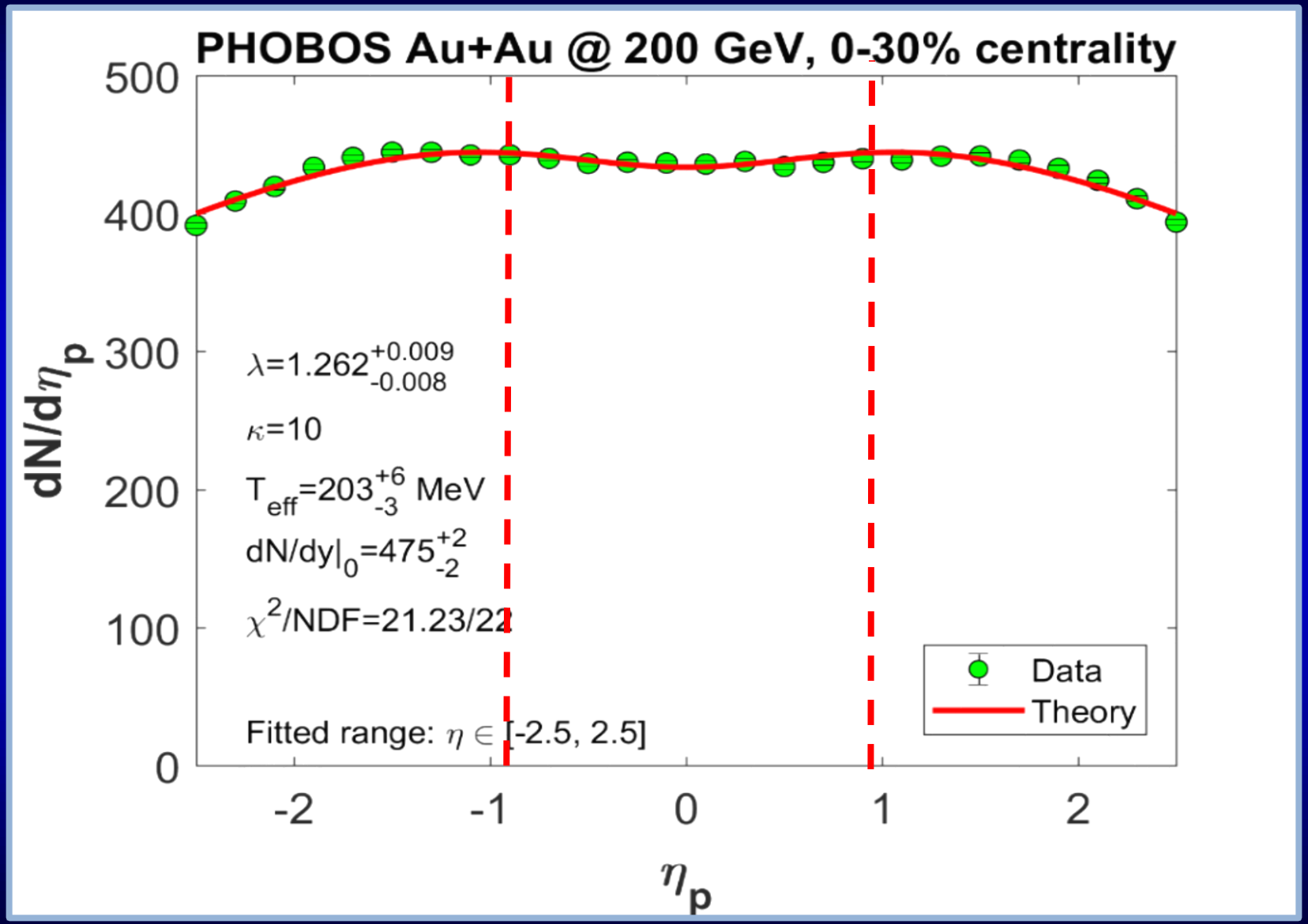

dn/dη fits, $\sqrt{s_{NN}}$ = 130 GeV

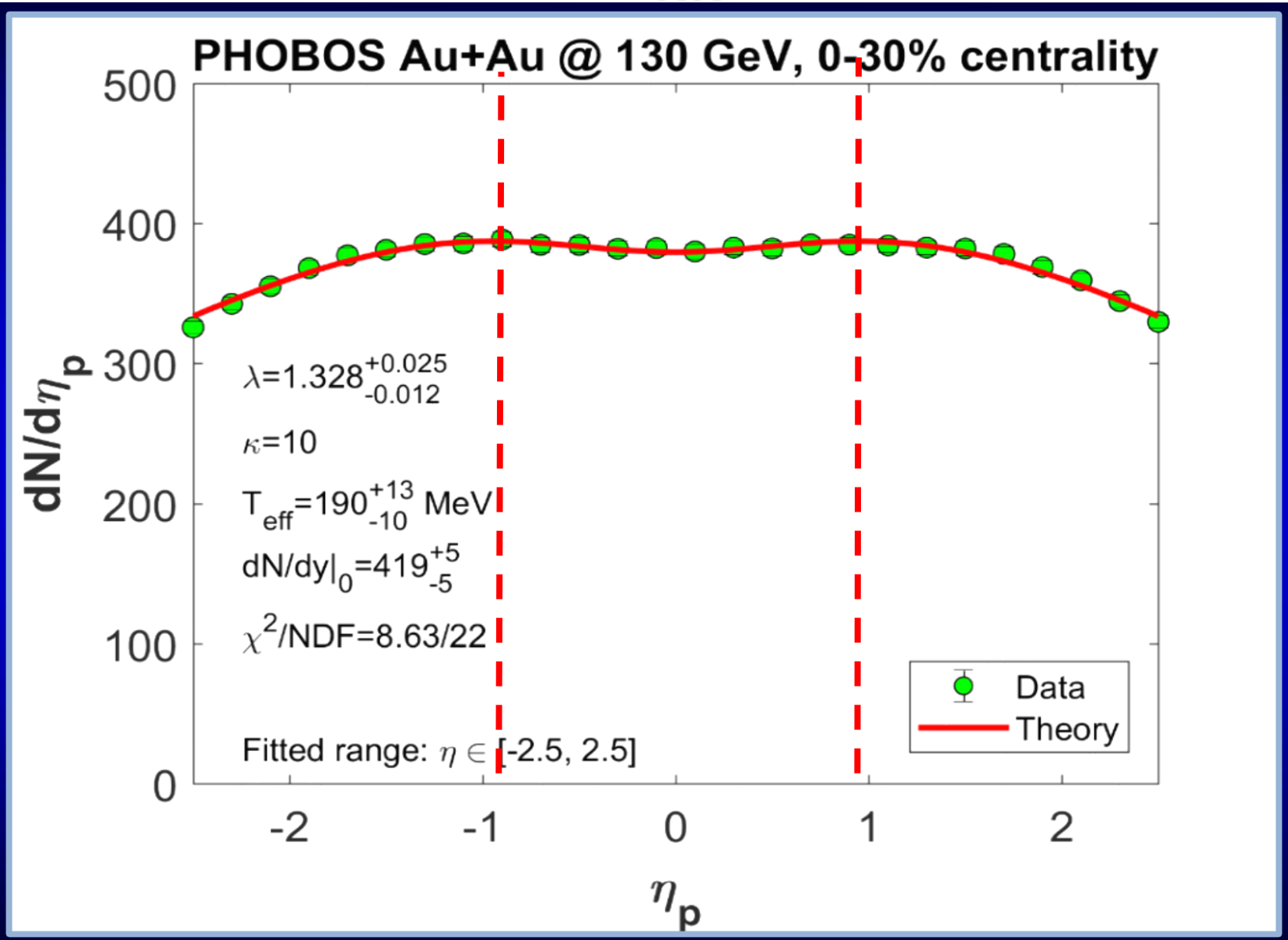

dn/dη fits, $\sqrt{s_{NN}}$ = 62.4 GeV

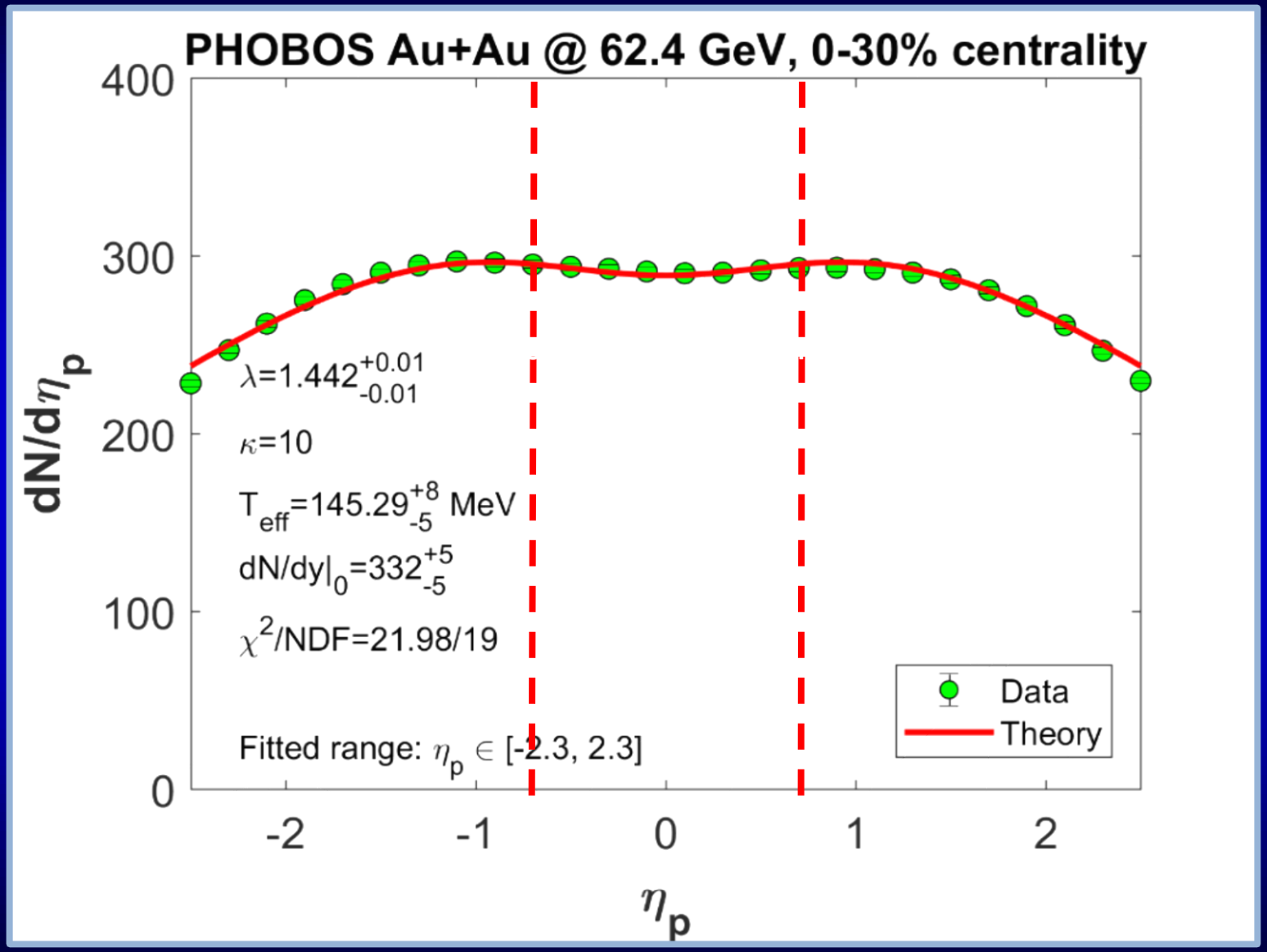

dn/dη fits, $\sqrt{s_{NN}}$ = 19.6 GeV

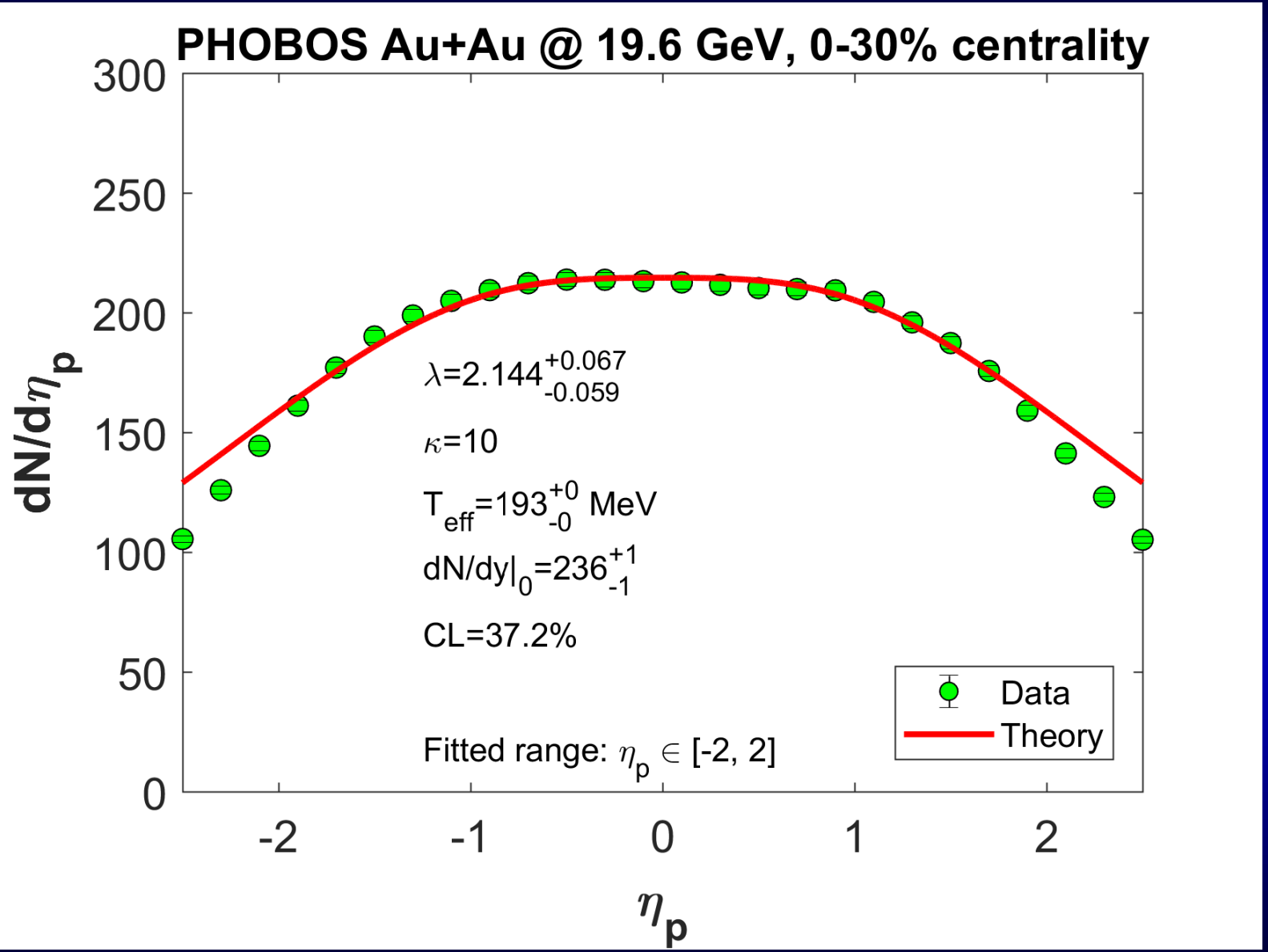

Rlong fits, $\sqrt{s_{NN}}$ = 62-200 GeV

$$R_L = \tau_f \Delta\eta_x \approx \frac{\tau_f}{\sqrt{\lambda\,(2\lambda-1)}}\sqrt{\frac{T_f}{m_T}}$$

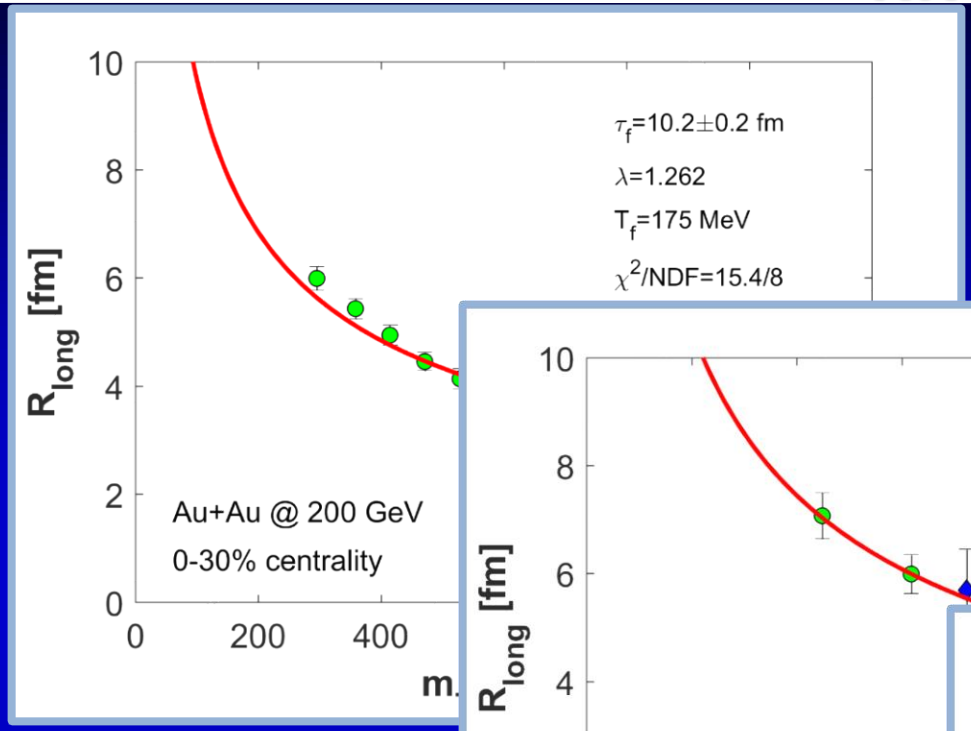

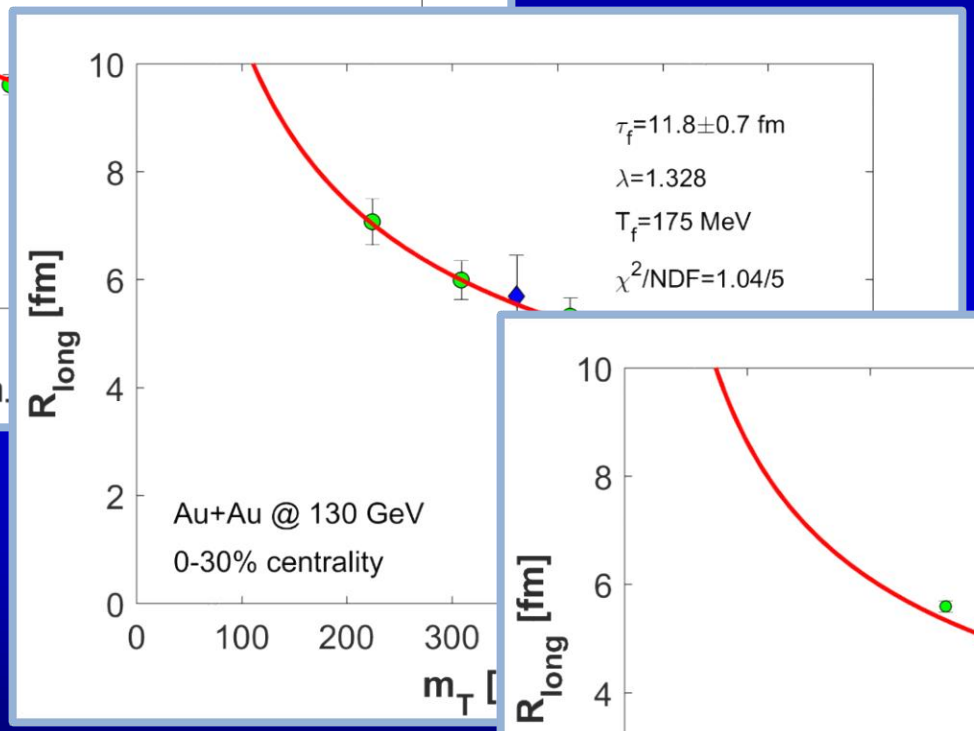

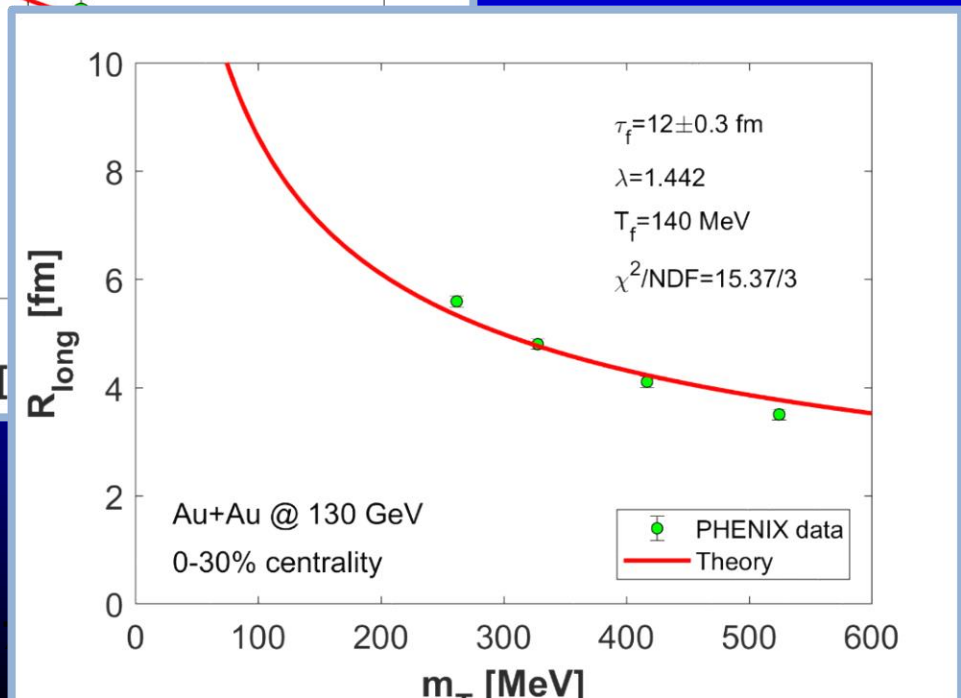

Correction factors, $\sqrt{s_{NN}}$ = 62-200 GeV

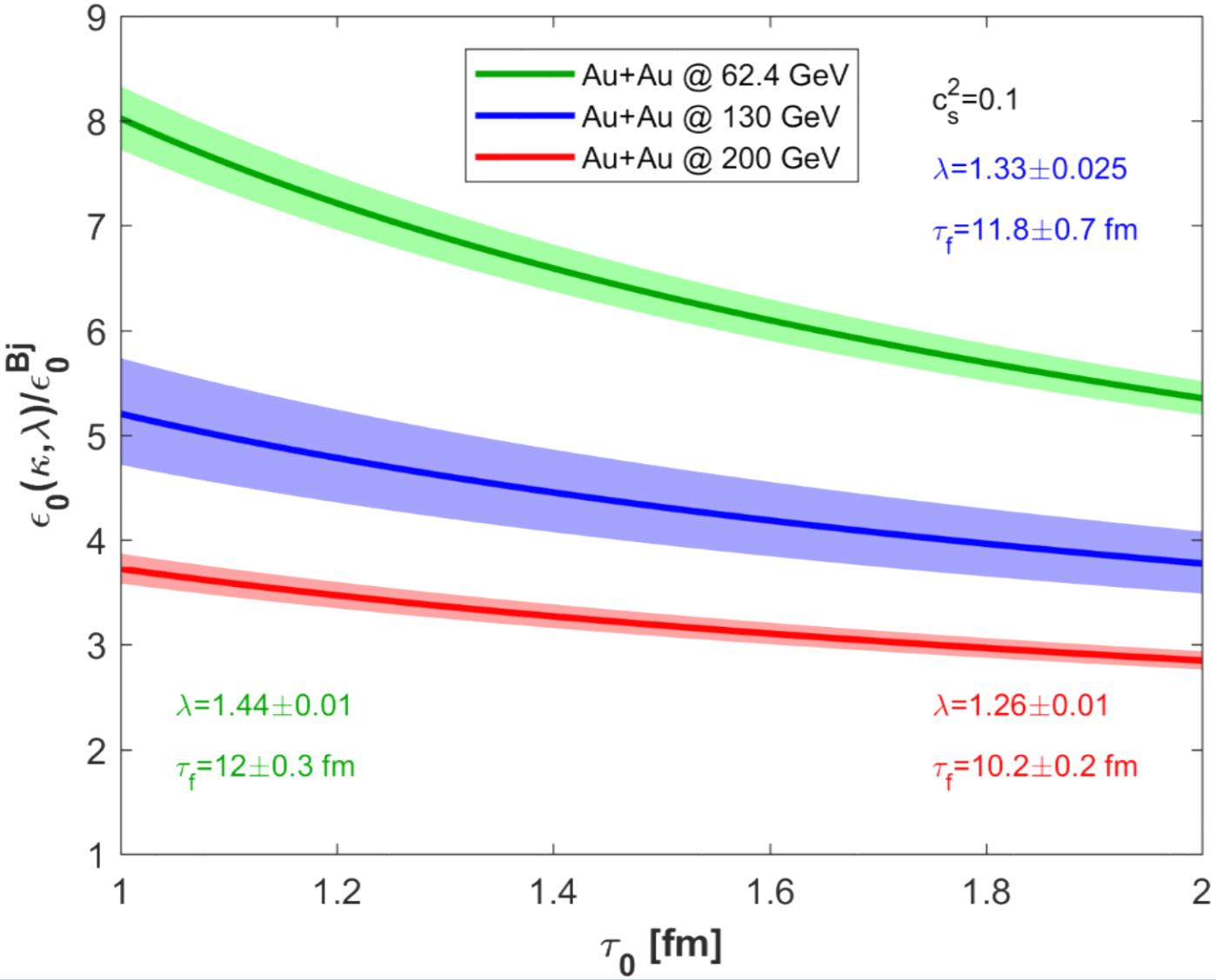

Init energy densities, $\sqrt{s_{NN}}$ = 62-200 GeV

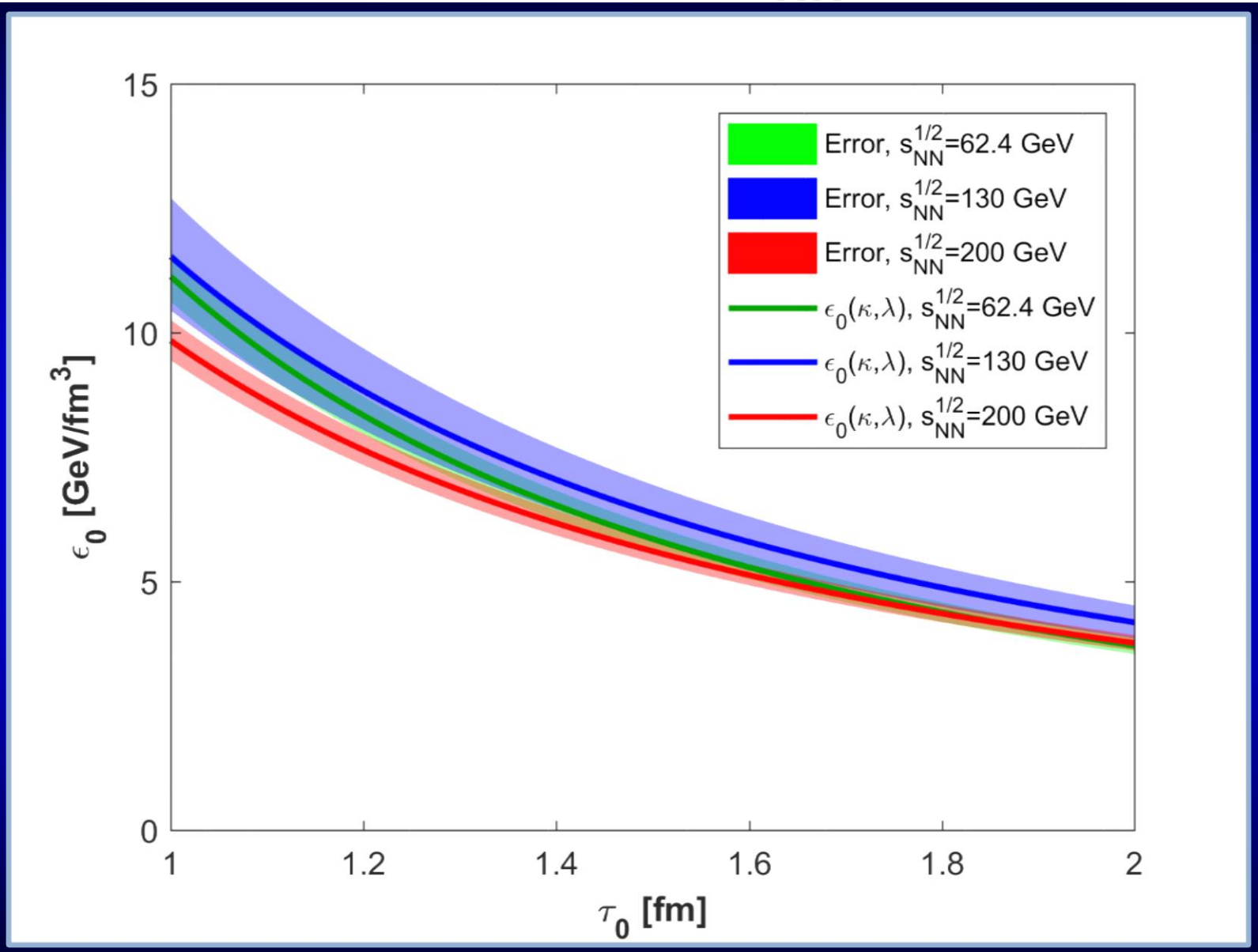

Conclusions

Explicit solutions of a very difficult problem

New estimates of initial energy density
New exact solution
for arbitrary EOS with const e/p
after 10 years, finally

Non-monotonic initial energy density(s)
A lot to do ...

more general EoS
less symmetry, ellipsoidal solutions
rotating viscous solutions
New solutions with shear/bulk viscosity ...

Thank you for your attention

Questions and Comments ?

Backup slides

Rlong systematics

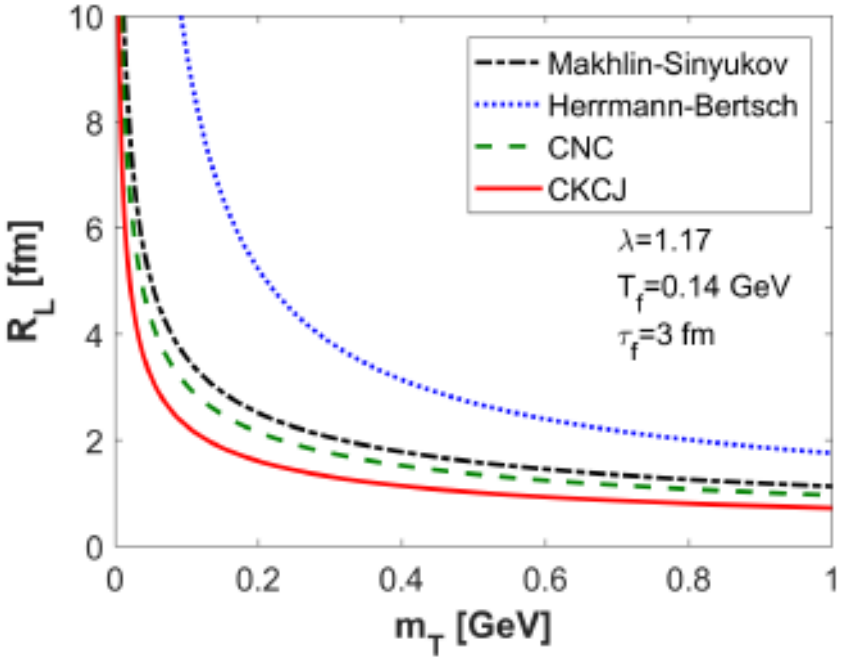

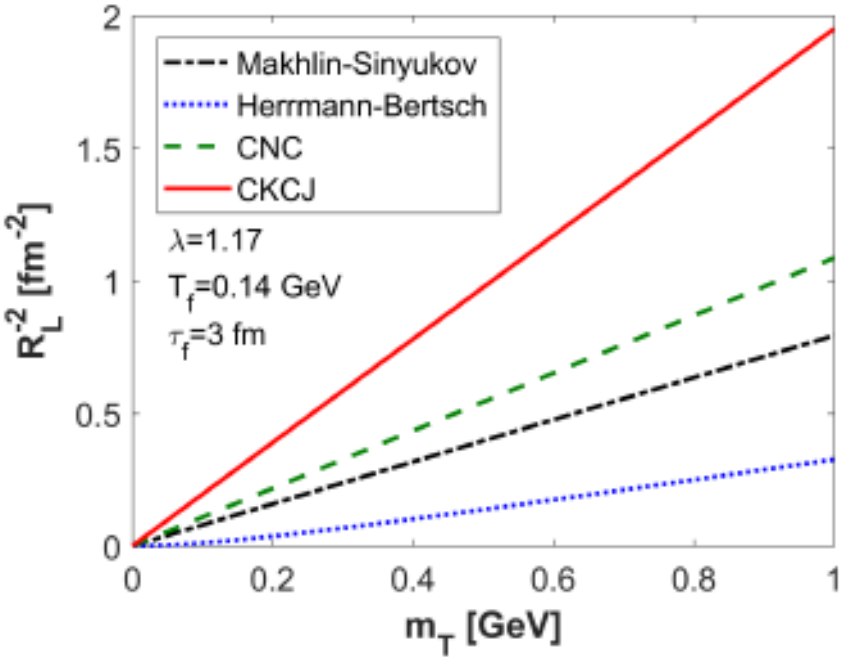

Fig. 2. The HBT radius $R_L(m_T)$ (left) and $1/R_L^2(m_T)$ (right) of the CKCJ solution are shown with solid red lines and compared to earlier estimations. The parameters correspond to fit results of the CKCJ solution to p+p collisions at $\sqrt{s} = 7$ TeV [2].

Teff systematics

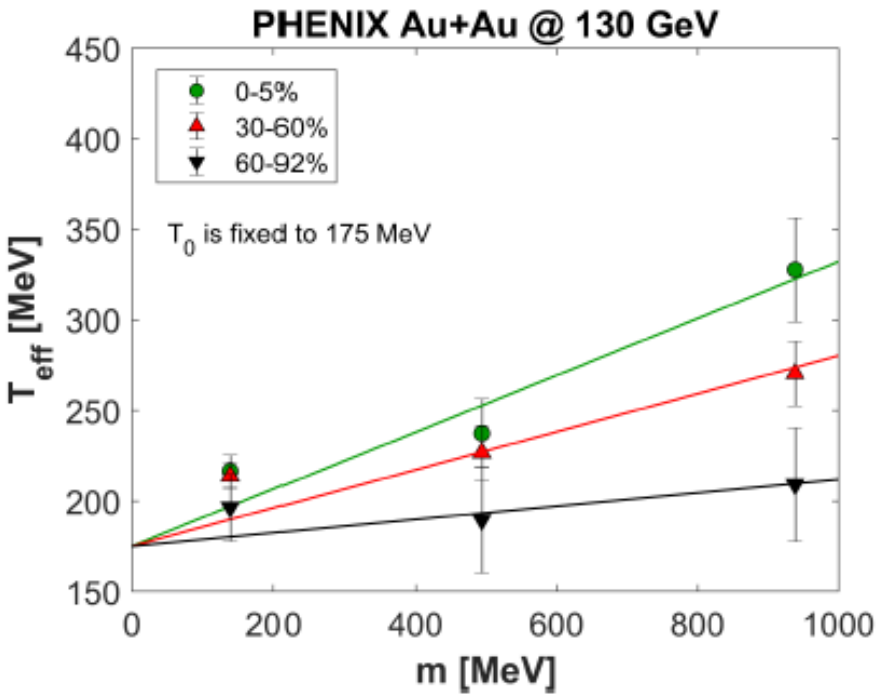

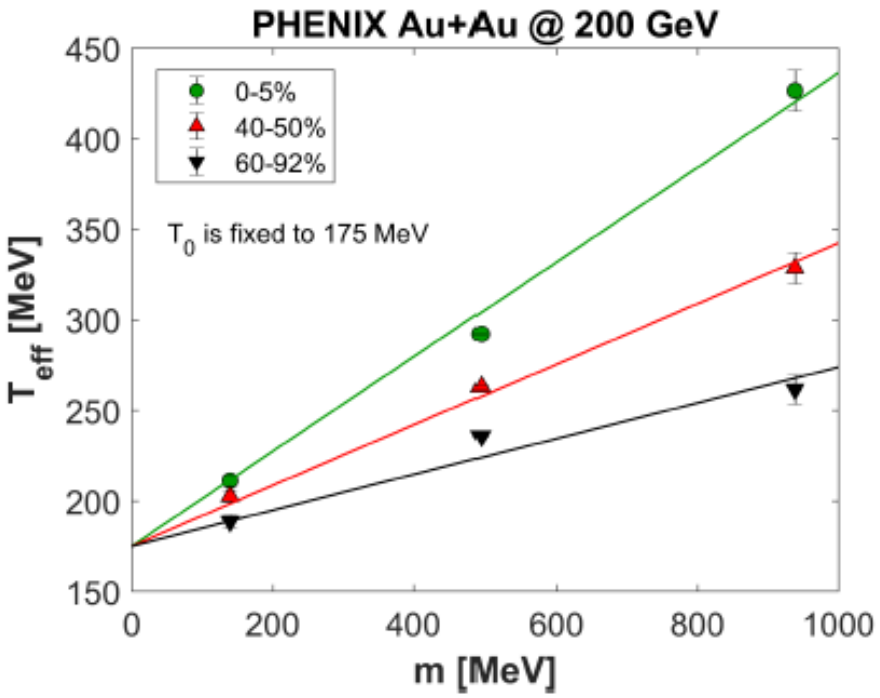

Figure 1. The mass and centrality dependence of the effective temperature of charged pions and kaons, as well as protons and anti-protons in $\sqrt{s_{NN}} = 130$ GeV and $\sqrt{s_{NN}} = 200$ GeV Au+Au collisions. For each centrality classes, the linear fits are shown by continuous lines. T_f is fixed to 175 MeV in both cases, although at 130 GeV, a slightly higher $T_f \approx 180$ MeV is preferred by the data.

dn/dη systematics

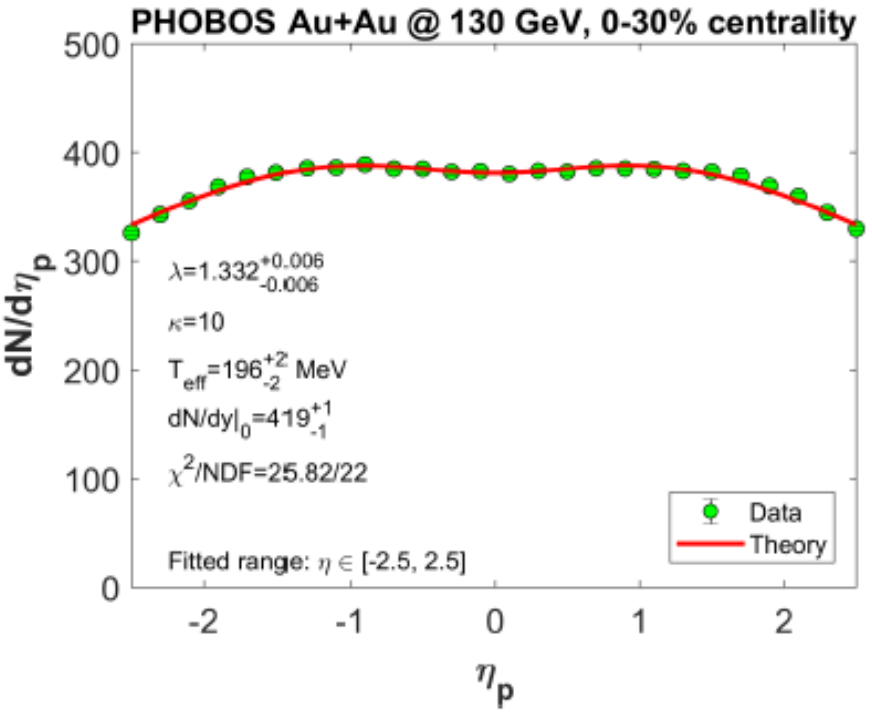

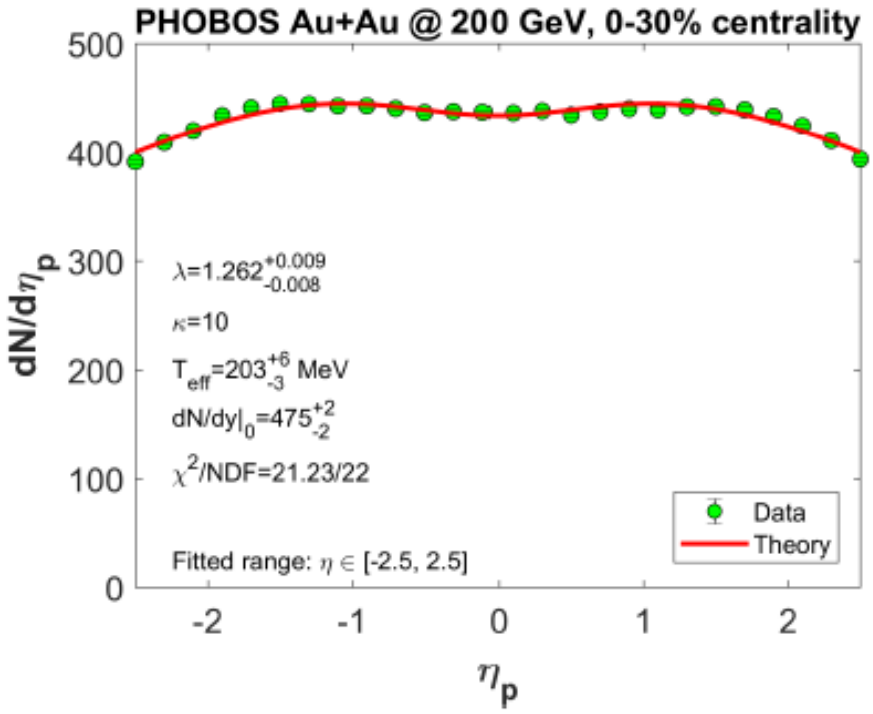

Figure 2. Fits of the pseudorapidity density with the CKCJ hydro solution [16], to PHOBOS Au+Au data at $\sqrt{s_{NN}} = 130$ GeV [24] (left) and $\sqrt{s_{NN}} = 200$ GeV [24] (right) in the 0-30 % centrality class. The speed of sound is $c_s^2 = 1/\kappa = 0.1$, fixed in both cases.

Rlong systematics

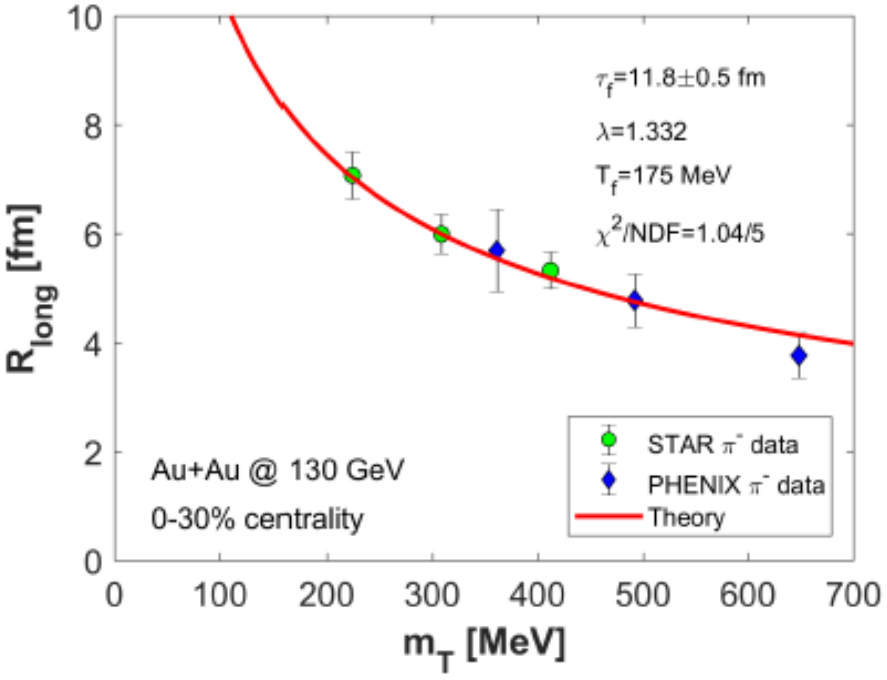

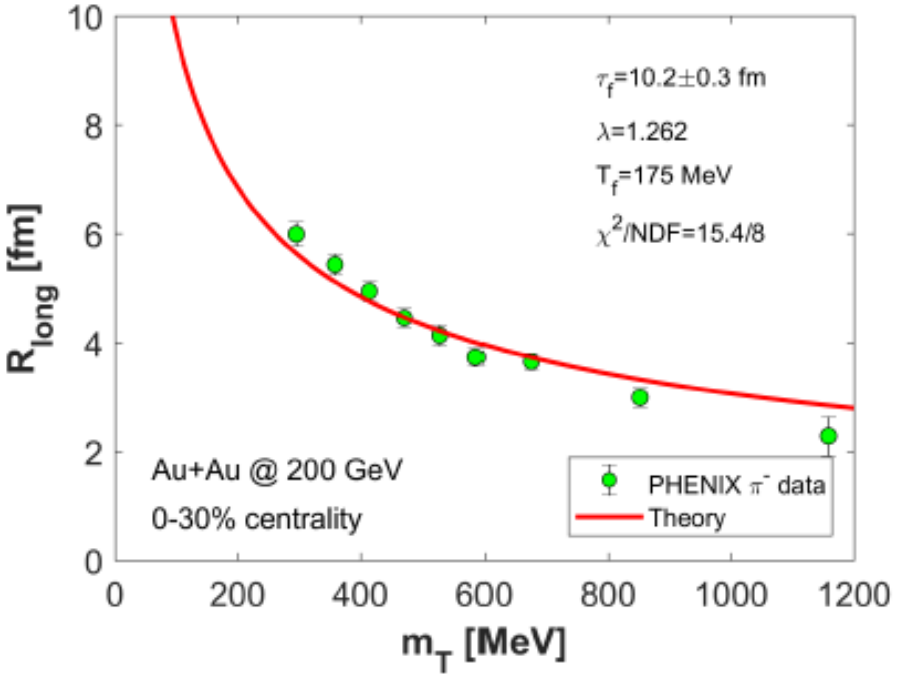

Figure 3. Fits of the longitudinal HBT-radii with the CKCJ hydro solution [16], to PHENIX and STAR Au+Au data at $\sqrt{s_{NN}} = 130$ GeV [28] (left) and to PHENIX Au+Au data at $\sqrt{s_{NN}} = 200$ GeV [29] (right) in the 0-30 % centrality class, for a fixed centrality, colliding energy and colliding system.

ε_0 systematics

Table 2. Initial energy density estimation from [31] by Bjorken's formula ε_0^{Bj}, and the conjectured values of $\varepsilon_0^{conj}(\kappa,\lambda)$, evaluated for $\tau_0 = 1$ fm/c . These values also indicate the non-monotonic behaviour of the initial energy density as a function of $\sqrt{s_{NN}}$, the center of mass energy of colliding nucleon pairs.

ε_0 [GeV/fm^3]	ε_0^{Bj}	$\varepsilon_0^{CNC}(\lambda)$	$\varepsilon_0^{conj}(\kappa,\lambda)$	$\varepsilon_0(\kappa,\lambda)$
Au+Au at 130 GeV, 6-15 %	4.1 ± 0.4	14.8 ± 2.2	11.2 ± 1.8	11.9 ± 0.5
Au+Au at 200 GeV, 6-15 %	4.7 ± 0.5	12.2 ± 2.3	9.9 ± 1.6	9.8 ± 0.4
Pb+Pb at 2.76 TeV, 10-20 %	10.1 ± 0.3	14.1 ± 0.5	13.3 ± 0.6	

$$\varepsilon_0(\kappa,\lambda) = \varepsilon_0^{Bj}(2\lambda-1)\left(\frac{\tau_f}{\tau_0}\right)^{\lambda\left(1+\frac{1}{\kappa}\right)-1},$$

$$\varepsilon_0^{Bj} = \frac{\langle E_T\rangle}{S_\perp \tau_0}\left.\frac{dN}{d\eta_p}\right|_{\eta_p=0}.$$

ε_0 systematics

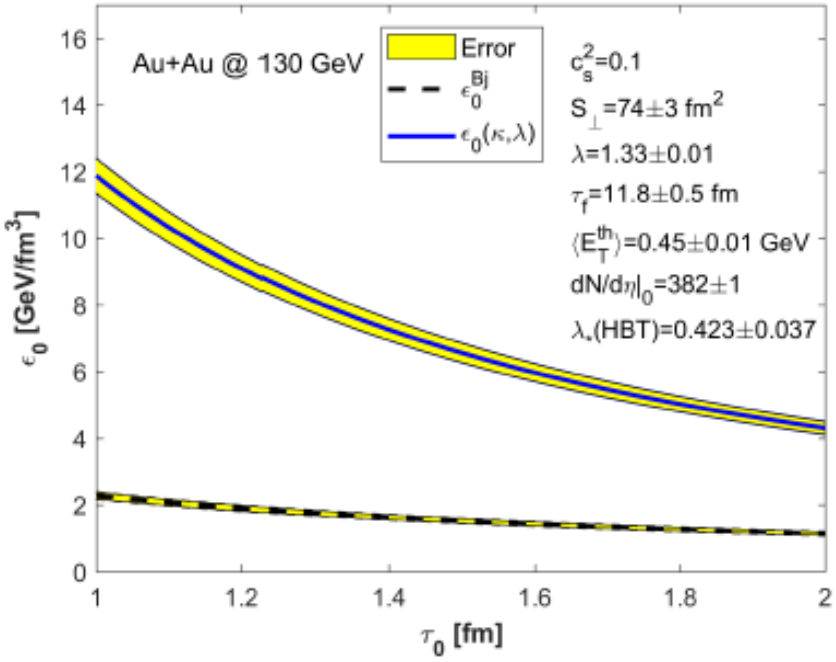

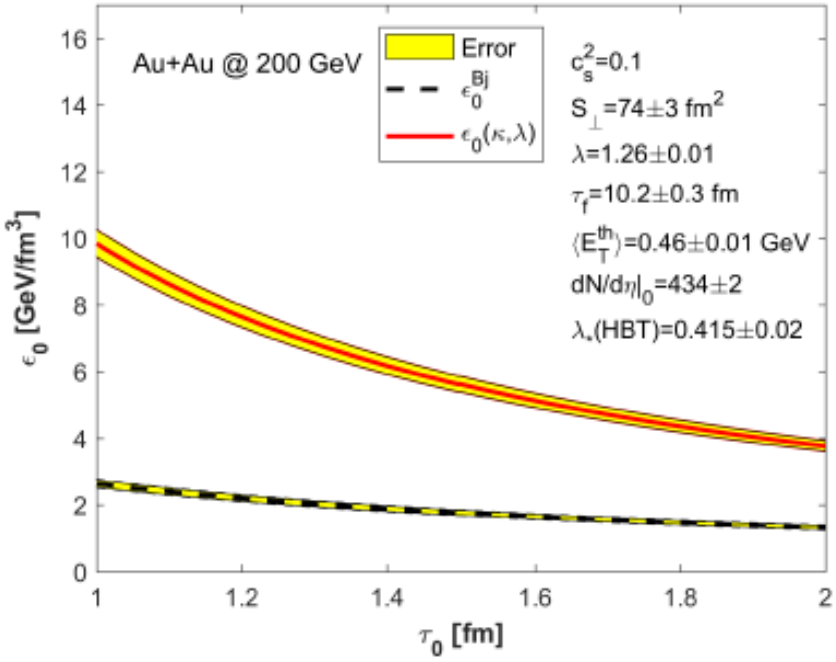

Figure 4. Initial energy density estimates from the CKCJ solution are shown with solid lines and compared to Bjorken's estimate, indicated with dashed lines, as a function of the initial proper time. The parameters of the left panel correspond to fit results of the CKCJ solution to PHOBOS Au+Au pseudorapidity density data in the 0-30 % centrality class both at $\sqrt{s_{NN}} = 130$ GeV (left panel) at $\sqrt{s_{NN}} = 200$ GeV (right panel).

$$\varepsilon_0(\kappa,\lambda) = \varepsilon_0^{Bj}(2\lambda-1)\left(\frac{\tau_f}{\tau_0}\right)^{\lambda\left(1+\frac{1}{\kappa}\right)-1},$$

$$\varepsilon_0^{Bj} = \frac{\langle E_T\rangle}{S_\perp \tau_0}\left.\frac{dN}{d\eta_p}\right|_{\eta_p=0}.$$

ε_0 systematics

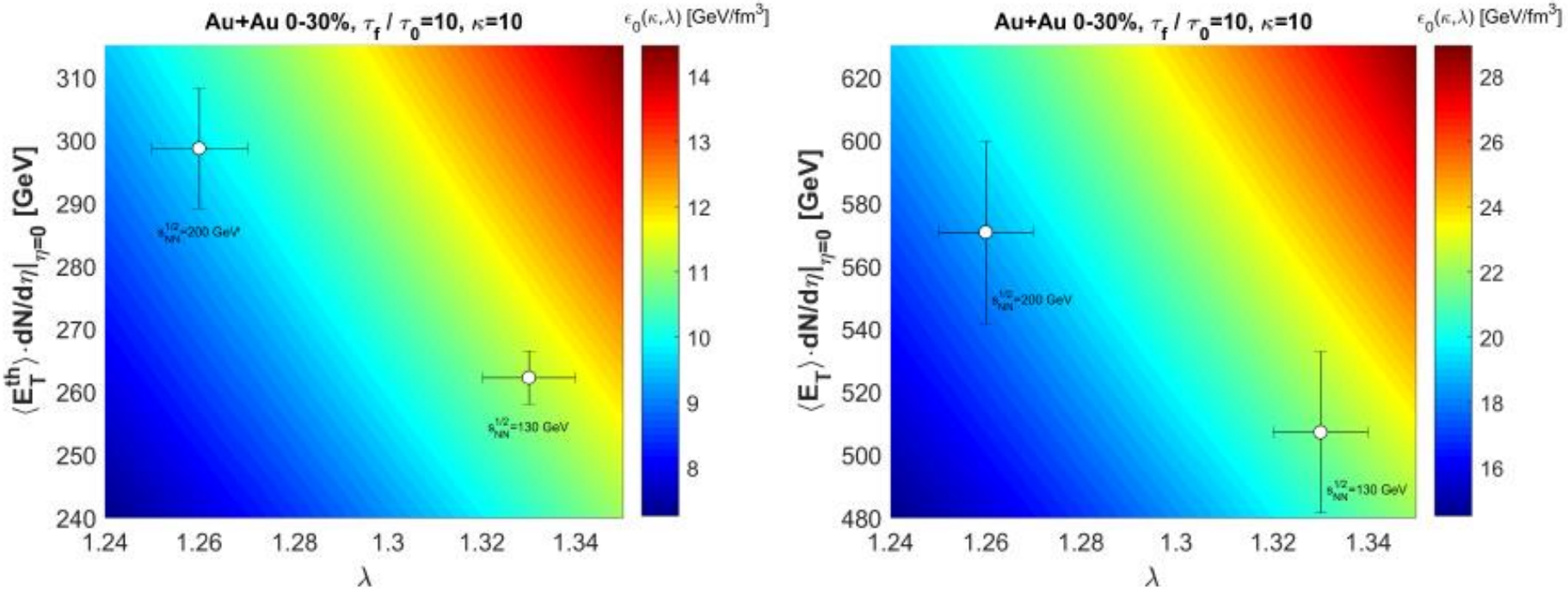

Figure 5. Location of the 0-30 % central Au+Au collisions on the $(\lambda, dE_T/d\eta_p)$ diagram for $\sqrt{s} = 130$ and 200 GeV. The color code indicates the contours of constant initial energy densities, evaluated for the realistic $\kappa = 10$ equation of state, corresponding to the measured speed of sound $c_s^2 \simeq 0.1$ in these reactions. Conservatively, these contours are evaluated for a $\tau_f/\tau_0 = 10$ ratio of the final over initial proper-time. The left panel indicates the thermalized energy density while the right panel indicates the pseudorapidity density of all transverse energy, including energy in non-thermal, high transverse momentum processes.

$$\varepsilon_0(\kappa,\lambda) = \varepsilon_0^{Bj}(2\lambda-1)\left(\frac{\tau_f}{\tau_0}\right)^{\lambda\left(1+\frac{1}{\kappa}\right)-1},$$

$$\varepsilon_0^{Bj} = \frac{\langle E_T\rangle}{S_\perp \tau_0}\frac{dN}{d\eta_p}\bigg|_{\eta_p=0}.$$

Time evolution systematics

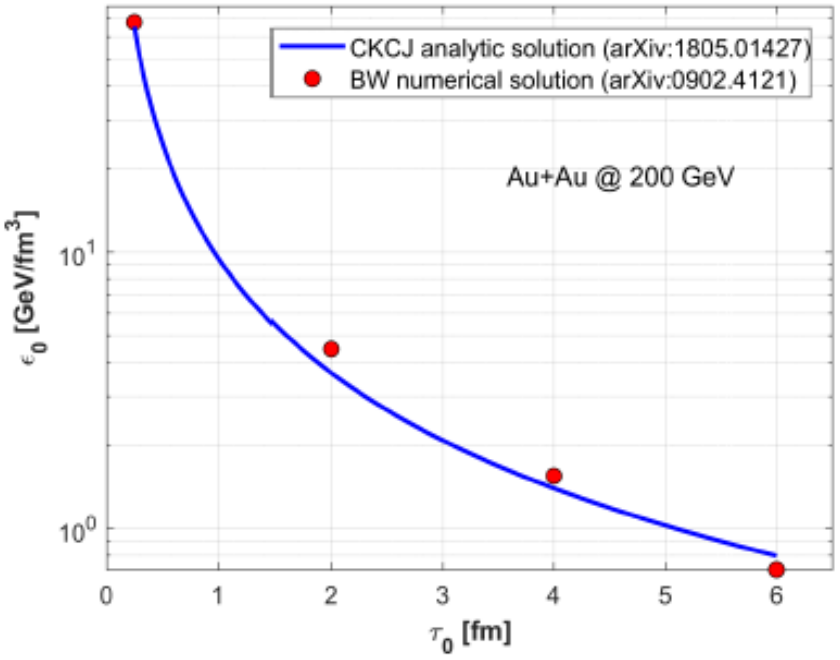

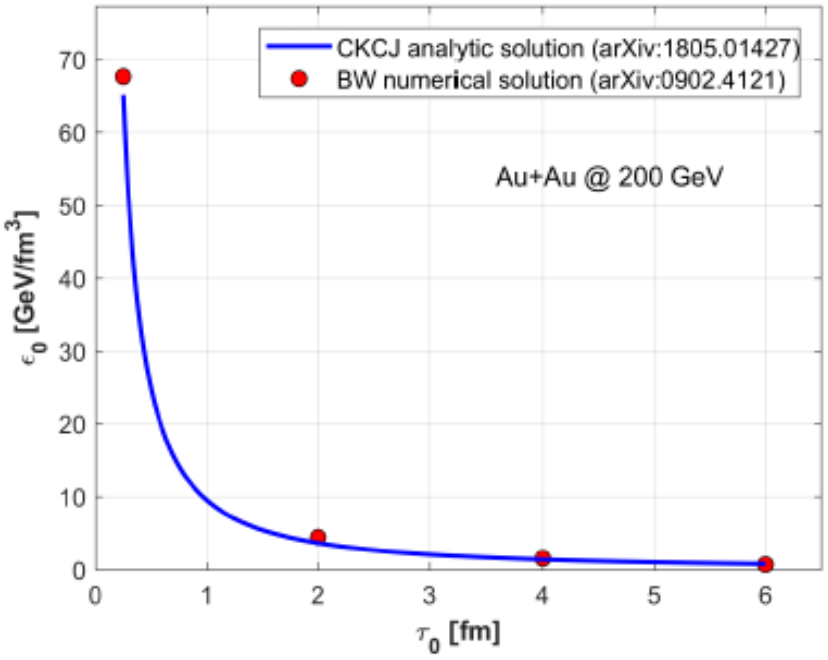

Figure 6. Initial energy density estimates from CKCJ analytic solution are show with blue solid lines and compared to the initial energy estimate from a numerical calculation of Bozek and Wyskiel [35], indicated with red markers, as a function of the initial proper time. The curves of the CKCJ analytic solution correspond to the solid red curves in the right panel of Fig. 4. The left panel shows the comparison with logarithmic vertical scale and the right panel shows the same with linear vertical scale.

$$\varepsilon_0(\kappa,\lambda) = \varepsilon_0^{Bj}(2\lambda-1)\left(\frac{\tau_f}{\tau_0}\right)^{\lambda\left(1+\frac{1}{\kappa}\right)-1},$$